Supporting Information

Self-assembly of Fmoc Protected Aliphatic Amino Acids to distinct tuneable morphologies

Bharti Koshti,[a+] Hamish W A Swanson,[b+] Basil Wilson [a], Vivekshinh Kshtriya,[a] Soumick Naskar, [a] Hanuman Narode,[a] King Hang Aaron Lau, [b] Tell Tuttle, [b] Nidhi Gour[a*]*

[a] Department of Chemistry, Indrashil University, Kadi, Mehsana, Gujarat, India; E-mail: gournidhi@gmail.com; nidhi.gour@indrashiluniversity.edu.in

[b] Department of Chemistry, University of Strathclyde, 295 Cathedral Street, Glasgow G1 1XL, United Kingdom Email: tell.tuttle@strath.ac.uk.

[+] Equal contribution

Methodology

Co-incubation study of Fmoc modified amino acids with microscopic dye

Co-incubation studies of Fmoc protected amino acids were done at both low and high concentration at room temperature and after heating at 70 ^{o}C with fluorescein and rhodamine B dyes. The final concentration of fluorescein and rhodamine B dye was 10 μM. A 20 μL solutions of this was drop casted on a clean glass slide and were visualized in fluorescent microscope under green and red filter.

Co-incubation study of Fmoc modified amino acids with urea

All Fmoc modified amino acids were co-incubated with urea at both low and high concentration. The co-incubation studies of Fmoc modified amino acids with urea were done at various ratios of urea such as 1:1, 1:3 and 1:5. A fixed concentration of Fmoc protected amino acid as 3mM was taken. A 20 μL solution of this was drop casted on a clean glass slide and visualized in Leica DM2500 upright fluorescent microscope under bright field mode.

Co-incubation study of Fmoc modified amino acids with tannic acid (TA)

The co-incubation study of Fmoc protected amino acids were done using various ratio of TA such as 1:1, 1:3 and 1:5 against modified amino acids. The images were visualized under

Leica DM2500 upright fluorescent microscope under bright filed with different magnification.

Solvent dependent analysis

The solvent dependent study was performed in tetrahydrofuran (THF) and methanol by using 50 mM stock solution of Fmoc protected amino acids dissolved in THF or methanol and then diluting it with appropriate solvent. Further, THF: water study was performed by increasing percentage of water from 10 to 90 % in THF.

UV-Visible spectroscopy studies

For UV-Visible study of all Fmoc protected amino acids, a 50 mM stock solution was prepared in methanol. Further dilution was carried out at final concentrations 5 μM, 10 μM, 25 μM, 50 μM, 75 μM, 100 μM using milli-Q water. The UV-visible spectra were recorded on Specord@270 plus, analytikjena, Germany.

Fluorescence Spectroscopy

The fluorescence spectra of Fmoc protected amino acids were recorded using JASCO FP8300 spectrofluorometer by giving excitation bandwidth 1 nm and emission bandwidth 2.5 nm respectively. The emission spectra of all Fmoc protected amino acids were recorded by diluting the 50 mM stock solution (in methanol) of modified single amino acids in milli-Q water to 50 μM and 100 μM final concentrations. The emission spectra were recorded by giving an excitation wavelength 290 nm and recording its emission in range of 300 to 600 nm.

X-Ray Diffraction (XRD)

X-ray diffraction experiments were performed on Bruker AXS D8 Focus P-XRD Bruker and AXS D8 VENTURE SC-XRD. All Fmoc protected single amino acids were evenly dispersed over the substrate holder and scanned in the range of 2θ 10-80°. The non-assembled samples (NA) used were commercially available. **FmocA** and **FmocI** used as such, while the assembled samples (SA) for XRD were prepared by lyophilizing 3mM solutions which were prior incubated for 24h at RT and thereafter lyophilized in Scale Bench Top Freeze Dryer.

Coarse Grained Molecular Dynamics (CG-MD)

Fmoc Model

The MARTINI Fmoc protecting group was produced according to the mapping scheme provided in (Figure S1). Bead types were selected to ensure a close relation to the model for phenylalanine in the MARTINI 2.1 forcefield.[1] Accordingly, a three to one mapping scheme was used with SC4 beads (mass 45 amu). To model the ester linkage a P5 bead was used (mass 72 amu). It is in this same manner that bonded terms were chosen. Improper dihedrals were defined between ring beads to ensure planarity and the equilibrium bond length between the two benzene rings are inequivalent (*e.g.*, the bond at the back was longer than at the front, which connects to the P5 beads) to produce a more triangle shape within the planar system. Previously we have reported good agreement between computational and experimental findings using this model.[2] Note, for the amino acids standard Martini 2.1. parameters were used.[1]

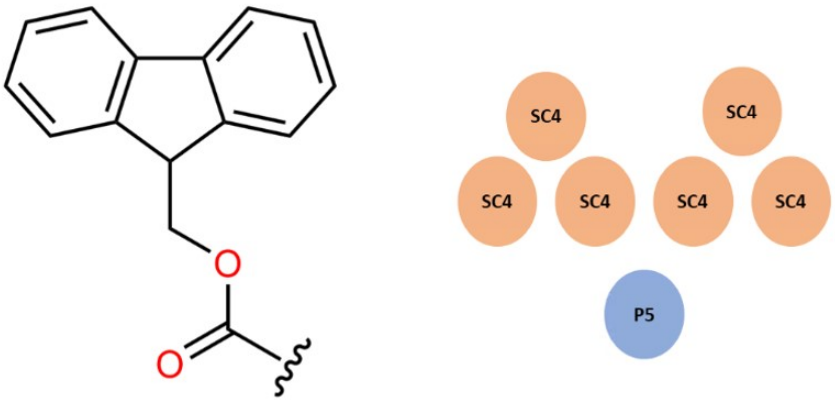

Figure S1. Atomistic representation of the Fmoc protecting group (left) and its MARTINI coarse grain bead representation with bead types shown (right).

Tetrahydrofuran model

Previously Patti *et al.* modelled THF using a single bead to represent THF in which the five heavy atoms are represented by a single 72 amu bead.[3] For this model, LJ parameters were refined via the interaction with octanol (C1 – P1) and water (P5) (Table S1) coined the 'TH' bead. However, no LJ parameters were selected for interaction with charged bead types, as these were not present within their system of interest.

Table S1 – LJ parameters for THF Model TH compared to an Na bead.

	Bead Type	ε (kJ mol^{-1})	σ (nm)

TH bead	TH – P4	4.120	0.480
	TH – C1	4.500	0.470
	TH – P1	2.700	0.470
Na bead	Na – P4	4.000	0.470
	Na – C1	2.700	0.470
	Na – P1	4.500	0.470

To avoid the need to reparametrize a new bead type for THF we consulted the Martini interaction matrix for version 2.1 and found that a Na bead would have the same interaction well-depth ε and interaction distance σ as the TH model for bead types C1 and P1. Notably, these were subtly different for the interaction with water P4, where the TH model has a well – depth of 4.12 kJ mol^{-1} and a σ value of 0.48.

To be confident in our representation of bead type, we evaluated the LogP of a Na bead via Umbrella Sampling using the same methodology used throughout the parameterization of the Martini forcefield. [4] A box containing 640 octanol molecules and 1280 Martini water beads was prepared and a bead was simulated at 0.1 nm internals from -1.9 nm to +1.9 nm with a restraining potential applied and force constant of 1000 kJ mol^{-1} nm^{-2}. Each box was simulated for 10 ns. A Potential of Mean Force (PMF) was then generated using the Weighted Histogram Analysis Method (WHAM) implementation in Gromacs (*g_wham*)[5] from which the LogP was then evaluated. This method was adapted from the Martini tutorial found here.[6]

It was determined that this choice of bead overestimated the LogP value by ~ 0.13 units which we deemed to be reasonable given the simplified nature of the coarse-grained potentials used within Martini 2.1. Furthermore, THF is not significantly polar so 'N' – apolar is a logical choice of bead and the 'acceptor' sub-type represents best its hydrogen bonding character.

Table S2 – LogP evaluated for Na bead type compared to experimental THF value.

LogP Experimental	Experiment Number	LogP (Na)
0.460	**1**	0.624
	2	0.474
	3	0.678

	Mean	0.592
	Standard Deviation	0.086

Furthermore, we performed simulations (1600 molecules for 100 ns) of selected Fmoc single amino acids (FmocL, FmocP and FmocV) in water (P4), methanol (P3) and THF (Na) to ensure this choice of bead conformed with our chemical expectations. Specifically, that assembly/aggregation would occur in water and not in methanol or THF. Screenshots of the simulations are shown in Figure S2 illustrating that these expectations were met with the selection of beads we made.

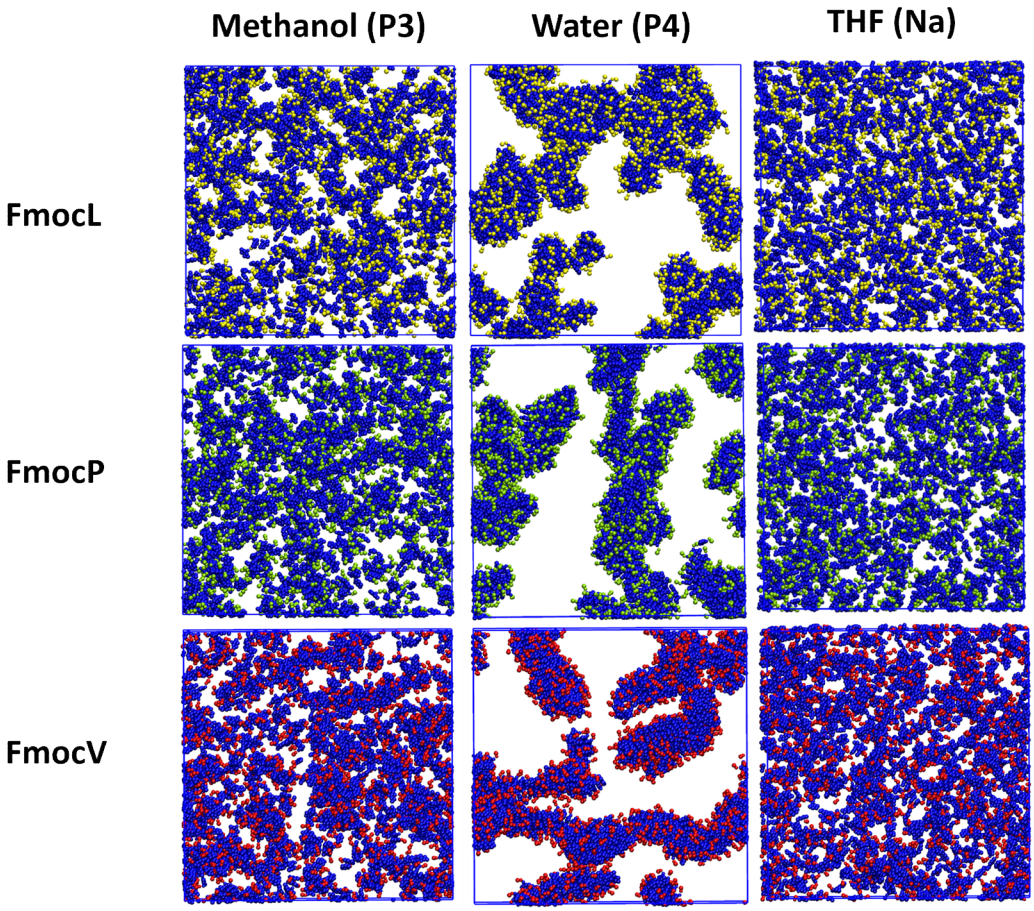

Figure S2. Screenshots of 1600 FmocL, FmocP and FmocV molecules in methanol (P3), water (P4) and THF (Na) after 100 ns. These simulations illustrate that the selection of an Na bead is appropriate for THF as no assembly occurs for molecules in this case, while it does in the presence of water (Note: blue beads represent Fmoc groups).

System Compositions

For each system 1600 molecules of a given Fmoc molecule (FmocL, FmocI, FmocA, FmocV and FmocP) were randomly inserted into a cubic box with dimensions 22 x 22 x 22 nm with a

minimum molecular separation of 3 Å. These were solvated with a total of 80000 solvent beads with varied compositions, selected to leverage the fact that one Martini water bead is equivalent to four water atoms while one THF bead represents only one molecule. For example, in a 50 % water: THF solution, there are 4.49 moles of H_2O to 1 mole of THF present. If the total number of solvent beads is conserved (80,000) then to obtain this same ratio, 37680 THF beads (1 molecule per bead) and 42320 water beads (4 molecules per bead) would be required. These compositions are detailed in Table S2. 10 % of the water component were antifreeze beads to prevent freezing of water as crystalline domains emerge which is a recognized issue with Martini force field version 2.1.[7] Simulations were performed both with neutral and charged C-termini, for the latter case an additional 1600 sodium ions were added to neutralize the charge of the system. All systems were build using Gromacs version 2020.7.[8] Visualization of simulation results was done using Visual Molecular Dynamics (VMD)[9] and analysis was done using the python package MDAnalysis.[10]

Table S3 – Simulation system compositions

Percentage Water (%)	No. THF beads	No. Water beads
0	80000	0
20	62450	17550
50	37680	42320
80	14560	65440

Simulation Details

All simulation systems were minimized for 10000 steps. Following this an NPT equilibration (250000 steps with a 20 fs timestep) was performed for 5 ns using a Berendsen pressure coupling (compressibility = 4.5×10^{-5} bar^{-1} and pressure = 1 atm) with velocity rescaling at a temperature of 298.15 K with a time constant for coupling of 1 ps. For the production simulation, a timestep of 25 fs was used for a total of 40000000 steps for 1 μs, an NPT ensemble was used using isotropic Parrinello-Rahman pressure coupling (compressibility = 4.5×10^{-5} bar^{-1}, pressure = 1 atm and a time constant for pressure coupling of 12 ps) and again velocity rescaling was used with a reference temperature of 298.15 K. Both electrostatic and Lennard Jones (LJ) potentials were shifted to a straight cutoff at 11 Å as consistent with Martini simulation methodology for dealing with non-bonded interactions[11].

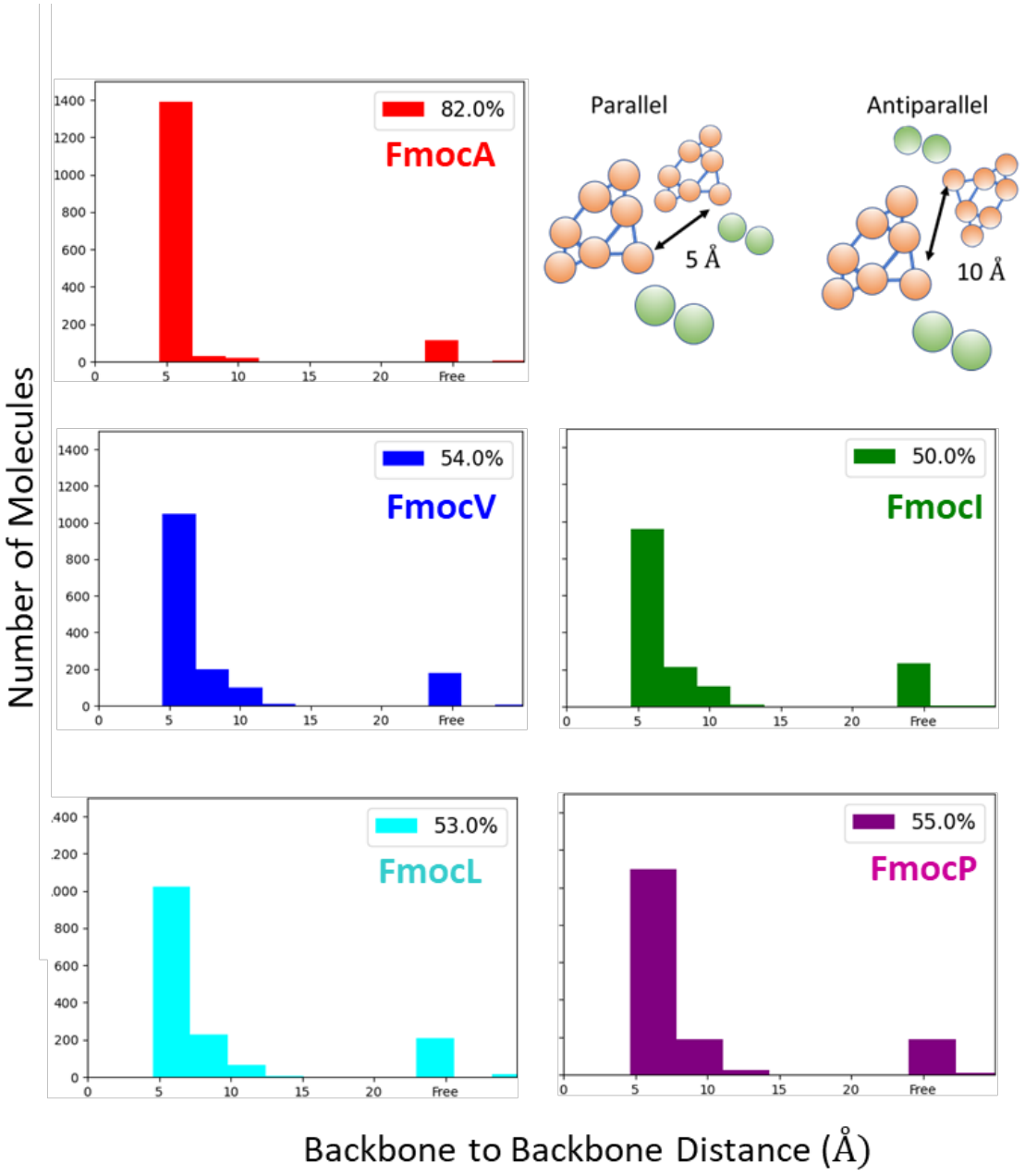

Figure S3. The number of parallel stacked Fmoc groups for neutral systems in 80 % water. As for the charged system this is highest for FmocA. For other aliphatic sequences, a range of spacings < 10 Å are found to be present in the assemblies. We hypothesise that steric and dispersive effects of the aliphatic sidechains disrupt homogenous stacking in these cases.

Microscopy Analysis

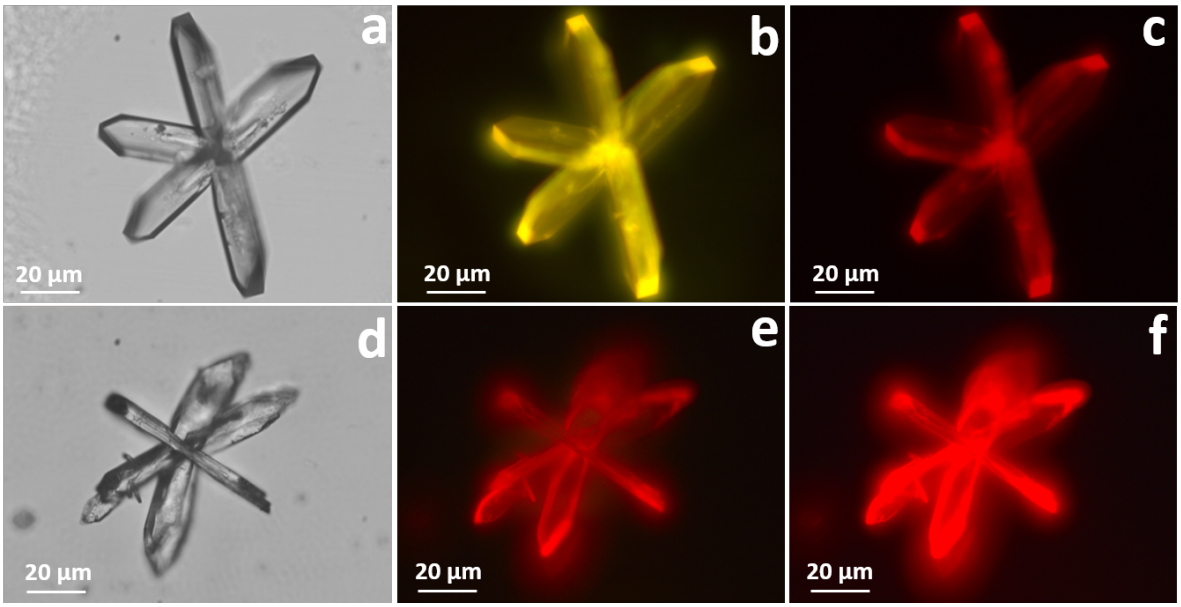

Figure S4: Microscopy images of 3 mM **FmocA** at RTwith dye (a) with 10 µM fluorescein dye under bright field; (b) with 10 µM fluorescein dye under green filter; (c) with 10 µM fluorescein dye under red filter; (d) with 10 µM rhodamine B dye under bright field; (e) with 10 µM rhodamine B dye under green filter; (f) with 10 µM rhodamine B dye under red filter

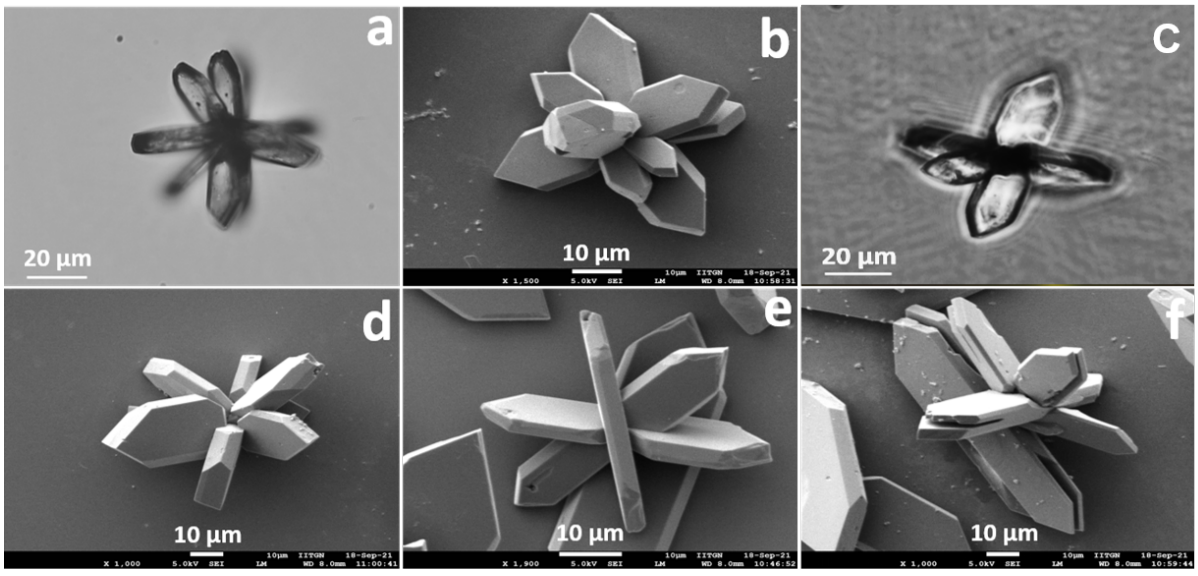

Figure S5: Self-assembled structures formed by **FmocA** (3 mM)**.** (a) Optical microscopy image under bright field at room temperature (RT); (b) FE-SEM image at RT; (c) Optical microscopy image at 8 mM under phase contrast; (d) FE-SEM image of 8 mM at RT; (e) FE-SEM image of 3 mM after heating at 70 ^{o}C; (f) FE-SEM image of 8 mM after heating at 70 ^{o}C.

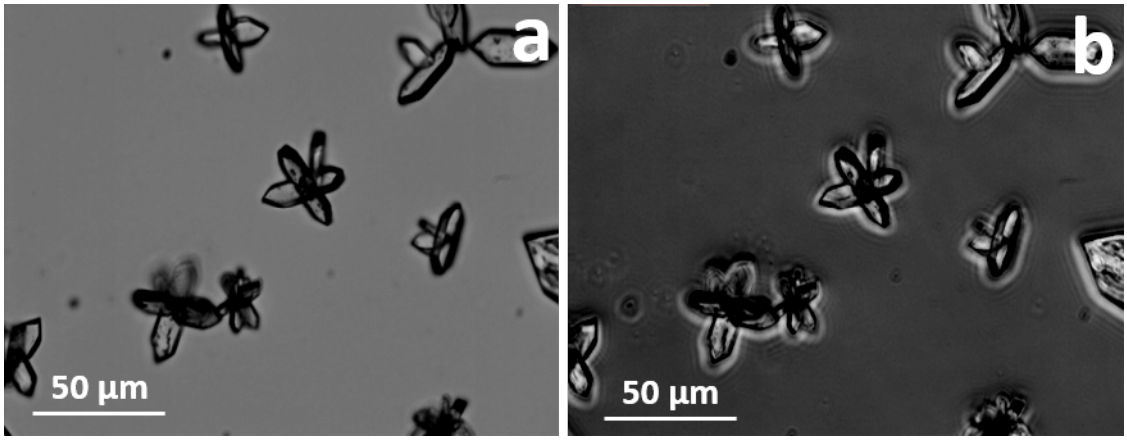

Figure S6: Microscopy images of 3 mM **FmocA** at RT (a) under bright field; (b) under phase contrast revealing crystalline characteristics as morphologies appeared bright in contrast to background.

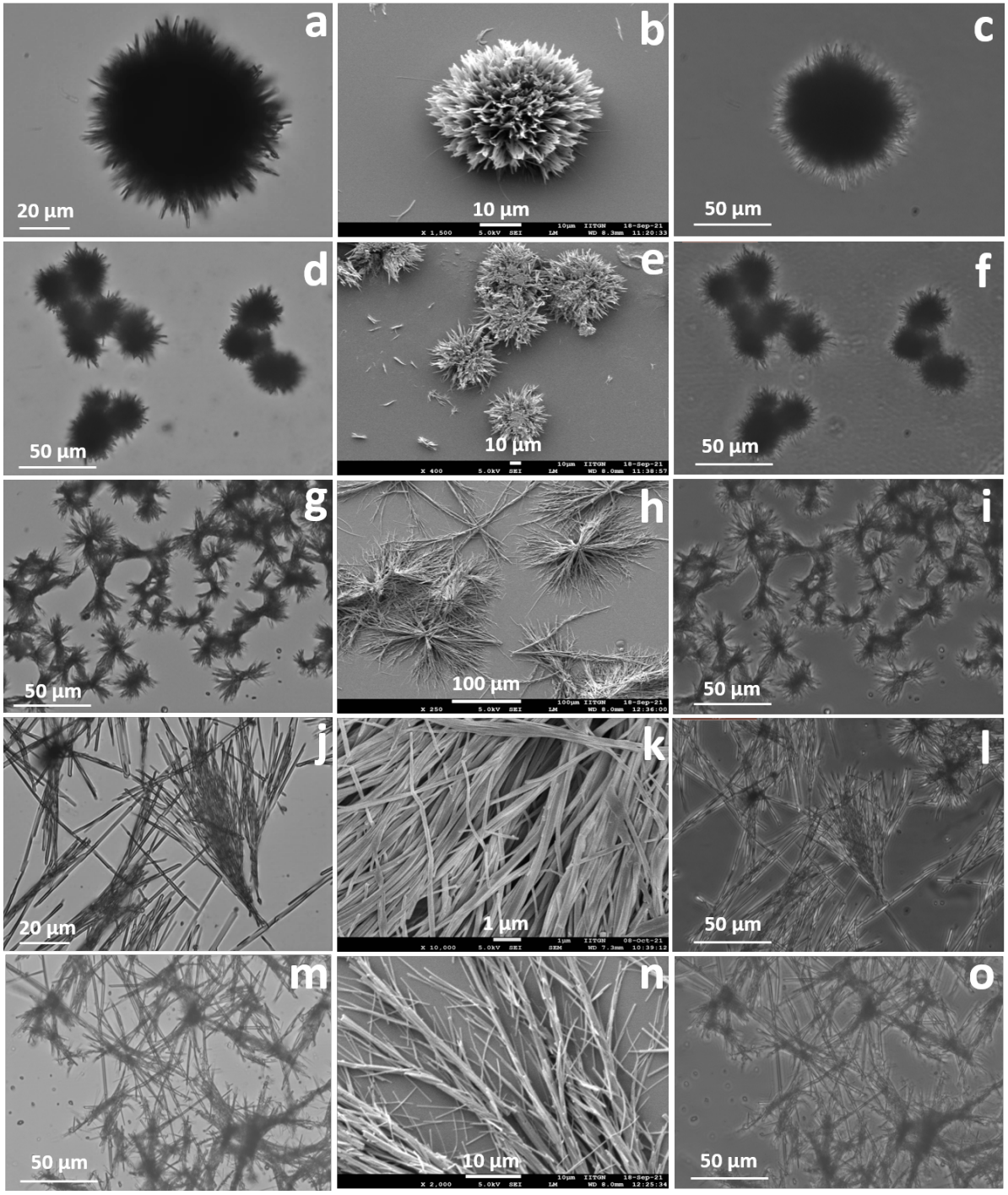

Figure S7. Concentration dependent morphological transitions in the self-assembly of **FmocV** at RT: (a) Optical microscopy image of 3 mM under bright field; (b) FE-SEM image of 3 mM; (c) Optical microscopy image of 3 mM under phase contrast; (d) Optical microscopy image of 5 mM under bright field ; (e) FE-SEM image at 5 mM(f) Optical microscopy image of 5 mM under phase contrast; (g) Optical microscopy image at 7 mM under bright field; (h) FE-SEM image at 7 mM; (i) Optical microscopy image of 7 mM under phase contrast (j) Optical microscopy image at 9 mM under bright field; (k) FE-SEM image at 9 mM;(l) Optical microscopy image of 9 mM under phase contrast; Self-assembled structure formed by **FmocV** after heating at 70 ^{0}C at 3 mM concentration (m) Optical

microscopy image under bright field; (n) FE-SEM image;(o) Optical microscopy image under phase contrast.

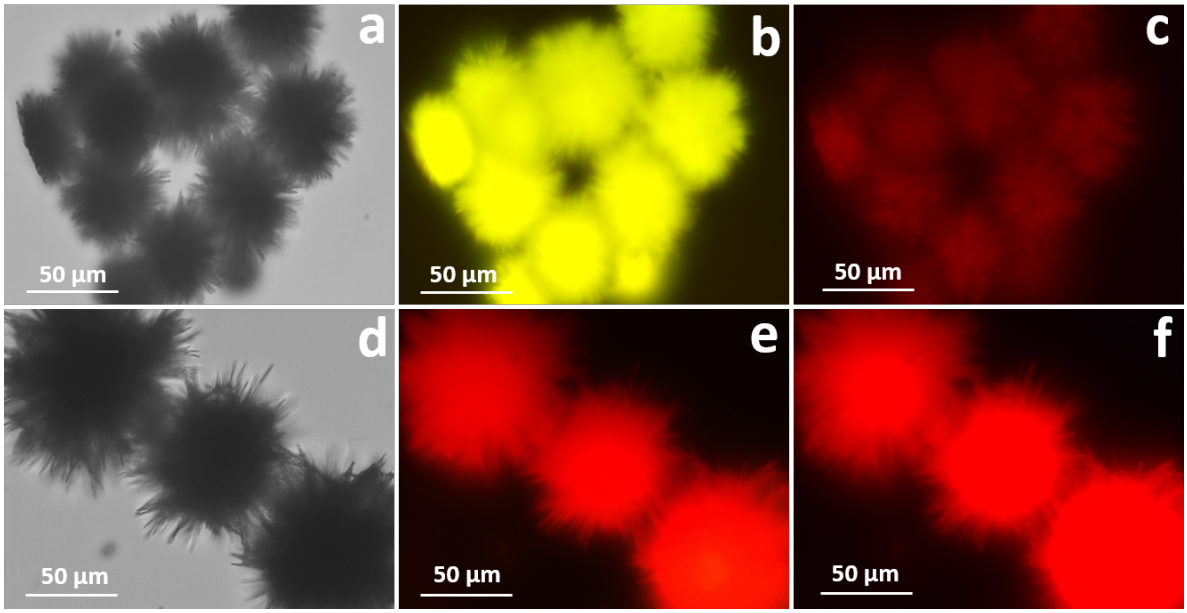

Figure S8: Microscopy images of 5 mM **FmocV** at RT with dye (a) with 10 µM fluorescein dye under bright field; (b) with 10 µM fluorescein dye under green filter; (c) with 10 µM fluorescein dye under red filter; (d) with 10 µM rhodamine B dye under bright field; (e) with 10 µM rhodamine B dye under green filter; (f) with 10 µM rhodamine B dye under red filter

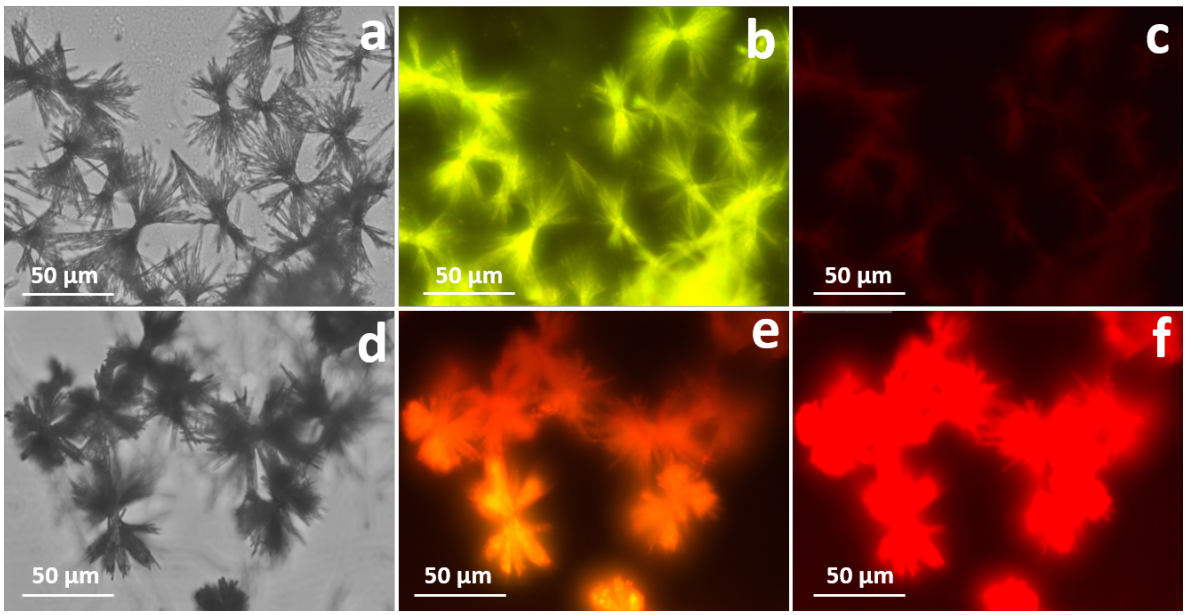

Figure S9: Microscopy images of 7 mM **FmocV** at RT with dye (a) with 10 µM fluorescein dye under bright field; (b) with 10 µM fluorescein dye under green filter; (c) with 10 µM fluorescein dye under red filter; (d) with 10 µM rhodamine B dye under bright field; (e) with 10 µM rhodamine B dye under green filter; (f) with 10 µM rhodamine B dye under red filter

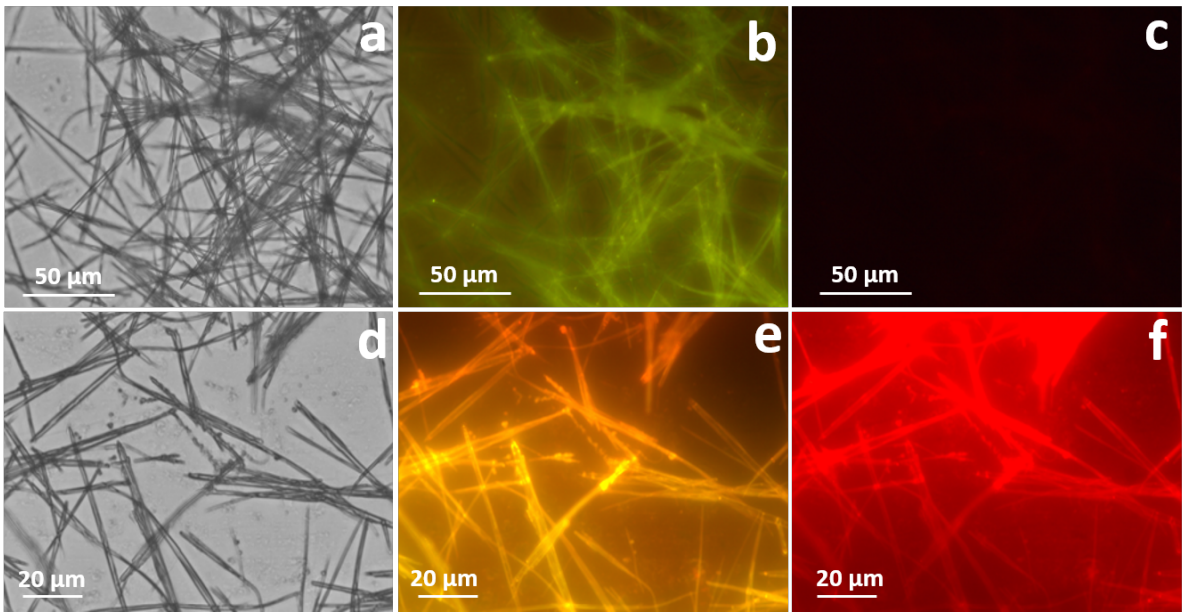

Figure S10: Microscopy images of 9 mM **FmocV** at RT with dye (a) with 10 µM fluorescein dye under bright field; (b) with 10 µM fluorescein dye under green filter; (c) with 10 µM fluorescein dye under red filter; (d) with 10 µM rhodamine B dye under bright field; (e) with 10 µM rhodamine B dye under green filter; (f) with 10 µM rhodamine B dye under red filter.

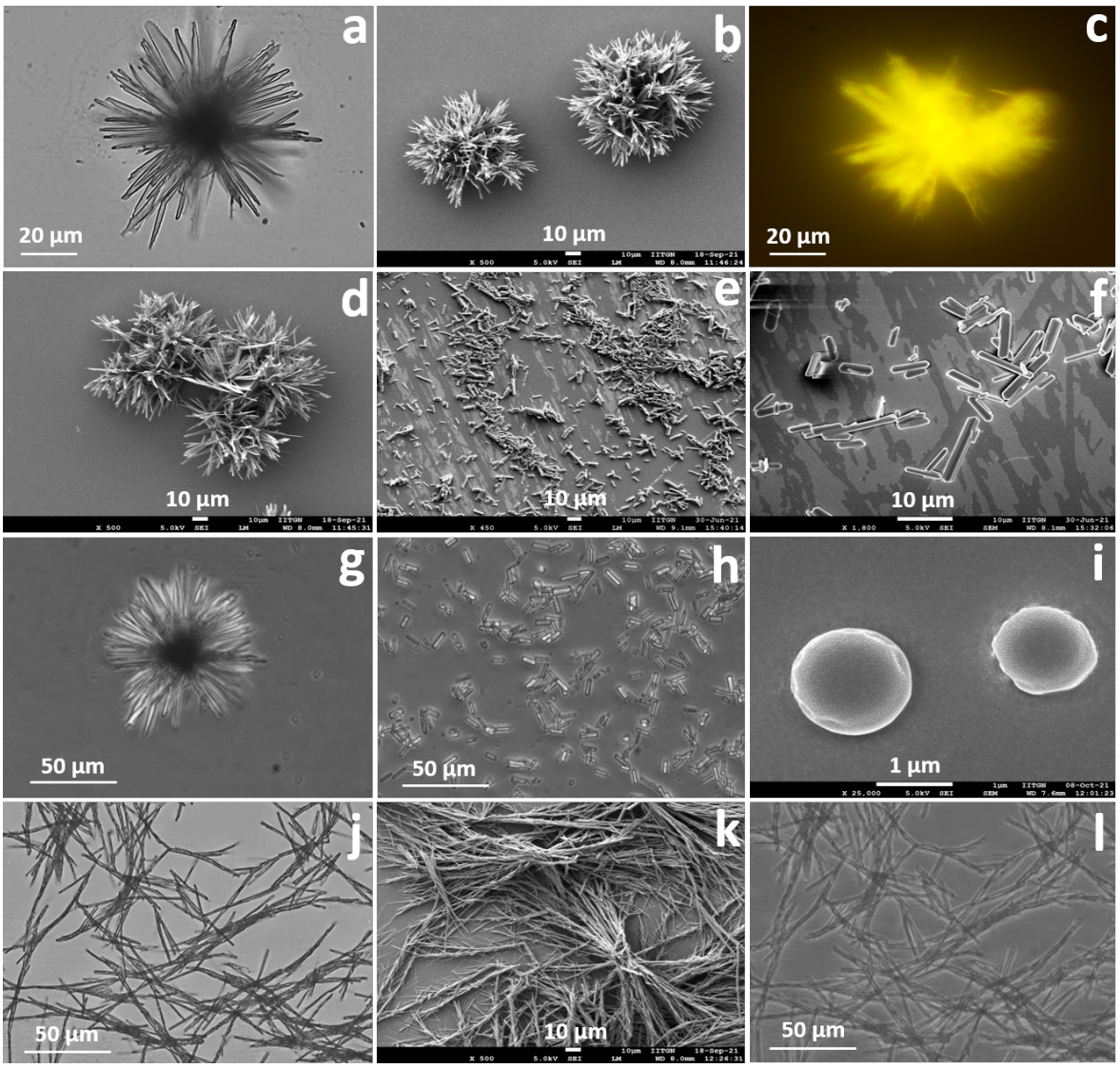

Figure S11. Self-assembled structure formed by **FmocL.** (a) Optical microscopy image of 3 mM under bright field at RT; (b) FE-SEM image of 3 mM at RT; (c) Fluorescence microscopy image of 3 mM fluorescein stained **FmocL** under green filter at RT; (d) FE-SEM image of 8 mM at RT; (e) FE-SEM image of 3 mM after heating at 70 °C; (f) FE-SEM image of 8 mM after heating at 70 °C; (g) Optical microscopy image of **FmocL (**3 mM) under phase contrast at room temperature (h) Optical microscopy image of **FmocL** (3 mM) under phase contrast after heating at 70 ^{0}C (i) FE-SEM image of **FmocL** (3mM) in methanol after heating at 70 ^{0}C; Self-assembled structure formation of **FmocI** (3 mM) at RT. (j) Optical microscopy image under bright field; (k) FE-SEM image; (l) Optical microscopy image under phase contrast.

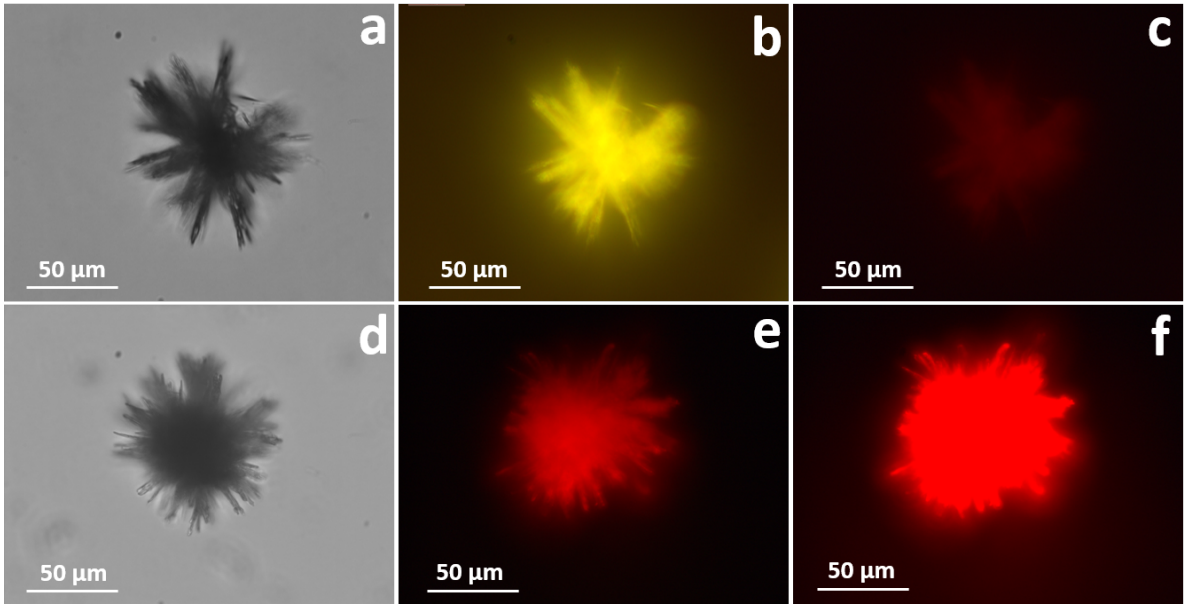

Figure S12: Microscopy images of **FmocL** at 3 mM under room temperature condition with microscopic dye (a) with 10 µM fluorescein dye under bright field; (b) with 10 µM fluorescein dye under green filter; (c) with 10 µM fluorescein dye under red filter; (d) with 10 µM rhodamine B dye under bright field; (e) with 10 µM rhodamine B dye under green filter; (f) with 10 µM rhodamine B dye under red filter.

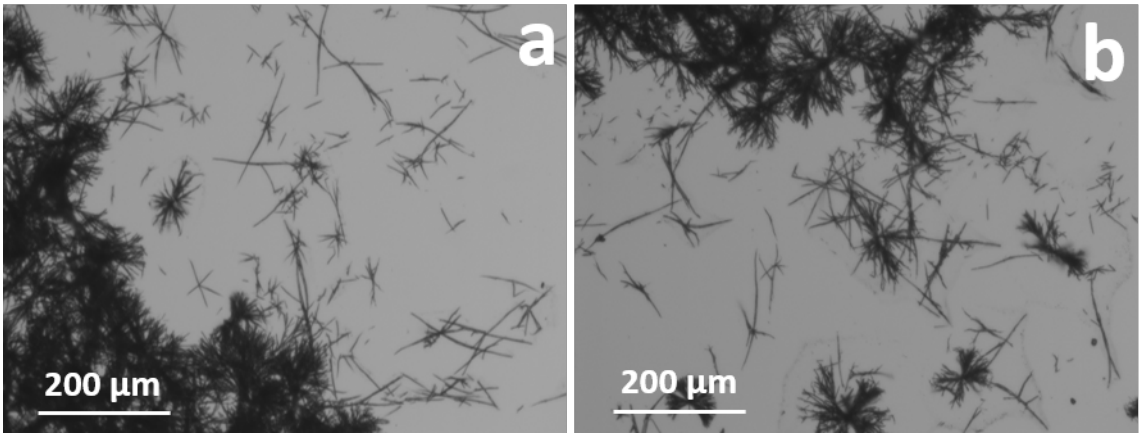

Figure S13: Optical microscopy images of **FmocI** at 3 mM after heating at 70 ^{0}C (a, b) Optical microscopy image under bright field

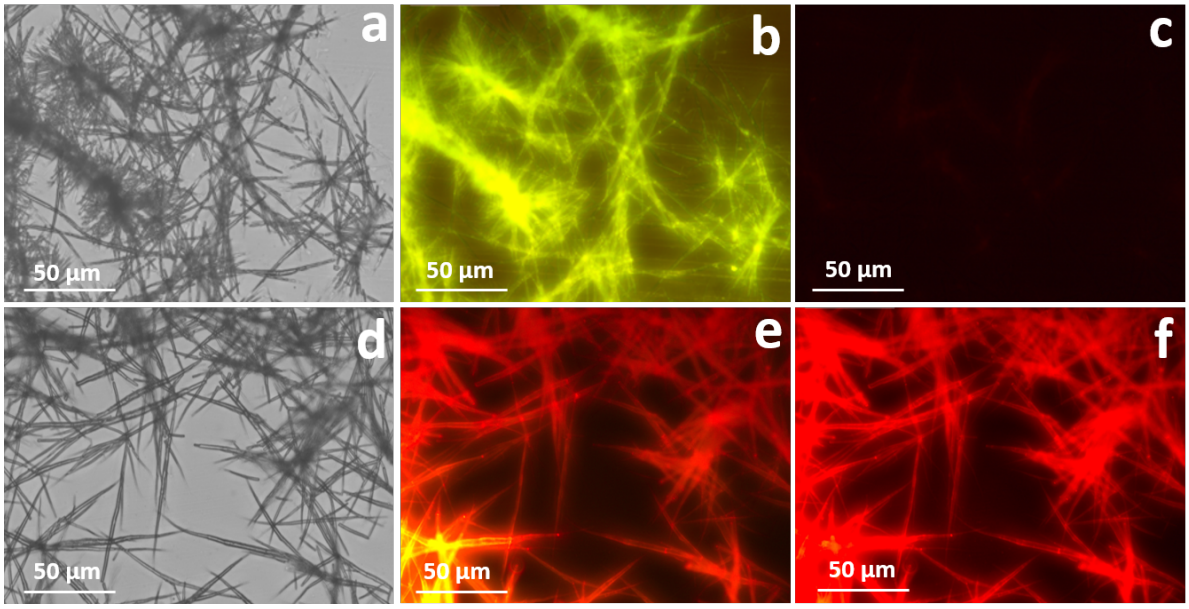

Figure S14: Microscopy images of **FmocI** at 3 mM under room temperature condition with microscopic dye (a) with 10 µM fluorescein dye under bright field; (b) with 10 µM fluorescein dye under green filter; (c) with 10 µM fluorescein dye under red filter; (d) with 10 µM rhodamine B dye under bright field; (e) with 10 µM rhodamine B dye under green filter; (f) with 10 µM rhodamine B dye under red filter.

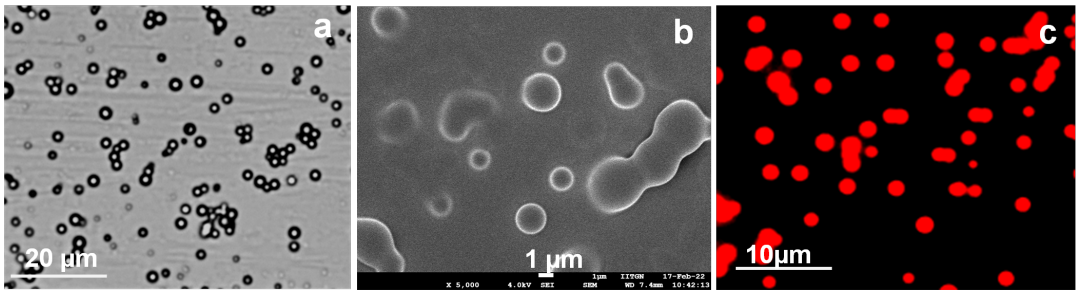

Figure S15: Microscopic images of **FmocP** at 3 mM under room temperature condition (a) optical microscopy; (b) SEM; (c) fluorescence microscopy with 10 µM rhodamine B dye under red filter.

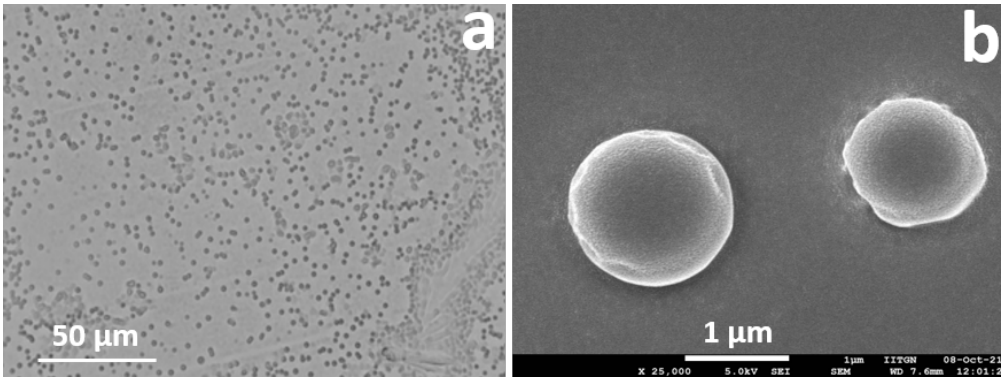

Figure S16: Microscopy images of **FmocL** in methanol after heating (a) Optical microscopy image under bright field; (b) FE-SEM image.

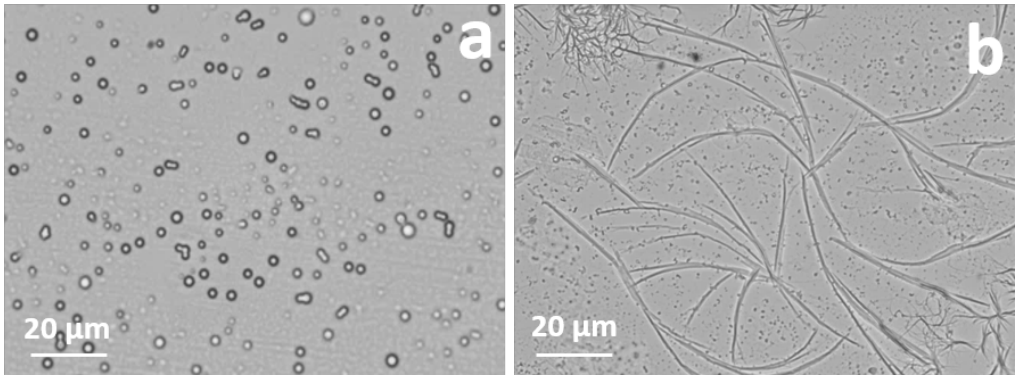

Figure S17: Microscopy images of **FmocP** (a) in 90% water:methanol at room temperature; (b) in methanol at room temperature.

Co-Incubation Studies

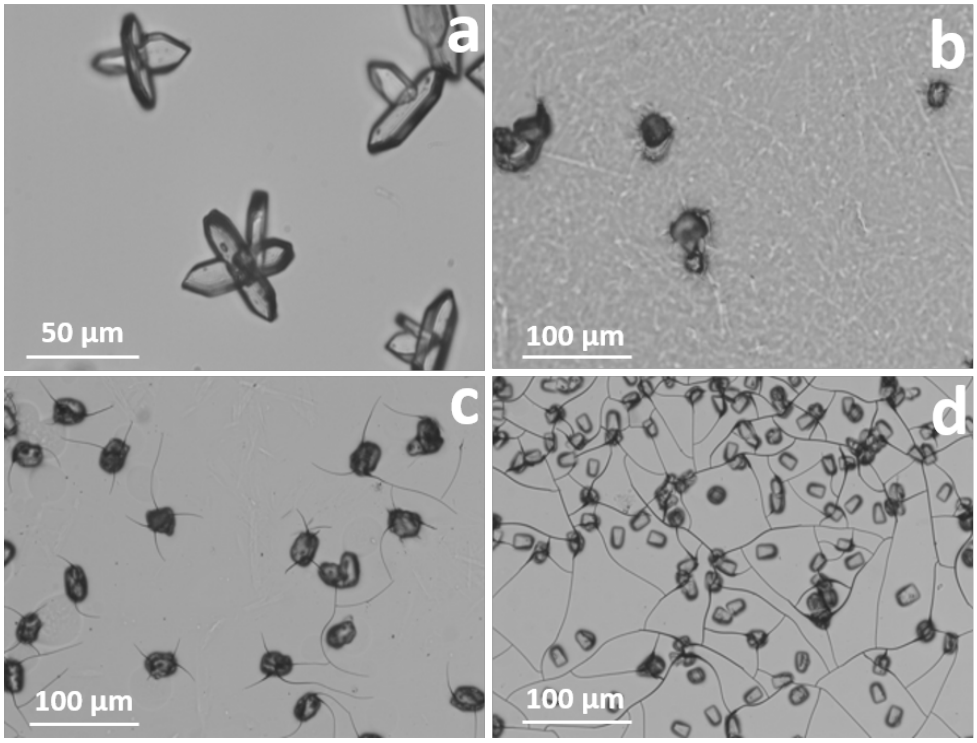

Figure S18: Microscopy images of **FmocA** at 3 mM concentration under room temperature when co-incubated with tannic acid. (a) **FmocA**at 3 mM under bright field; (b) with tannic acid 1:1; (c) with tannic acid 1:3; (d) with tannic acid 1:5.

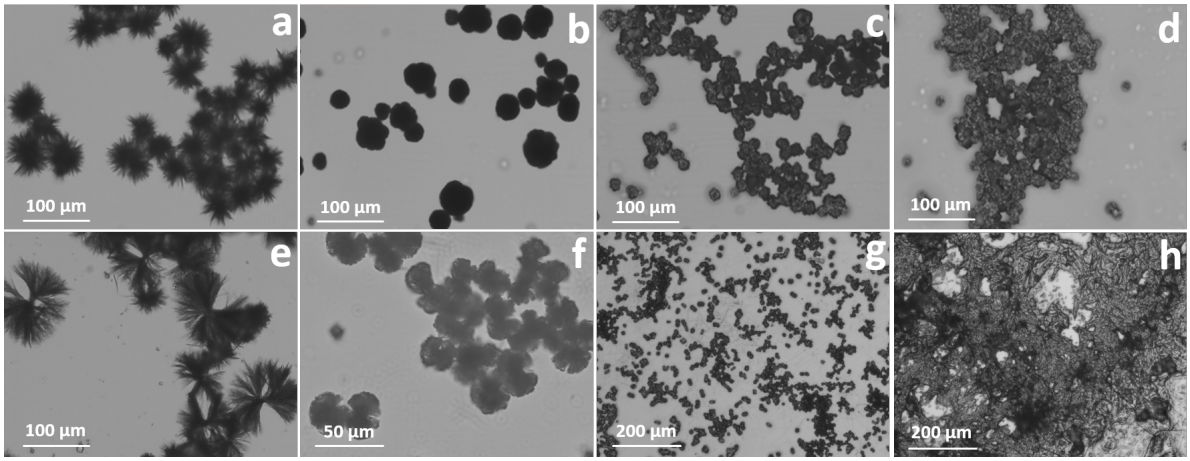

Figure S19: Microscopy images of **FmocV** under room temperature when co-incubated with tannic acid (a) **FmocV** at 5 mM under bright field; (b) at 5 mM with tannic acid 1:1; (c) at 5 mM with tannic acid 1:3; (d) at 5 mM with tannic acid 1:5; (e) **FmocV** at 7 mM under bright field; (b) at 7 mM with tannic acid 1:1; (c) at 7 mM with tannic acid 1:3; (d) at 7 mM with tannic acid 1:5

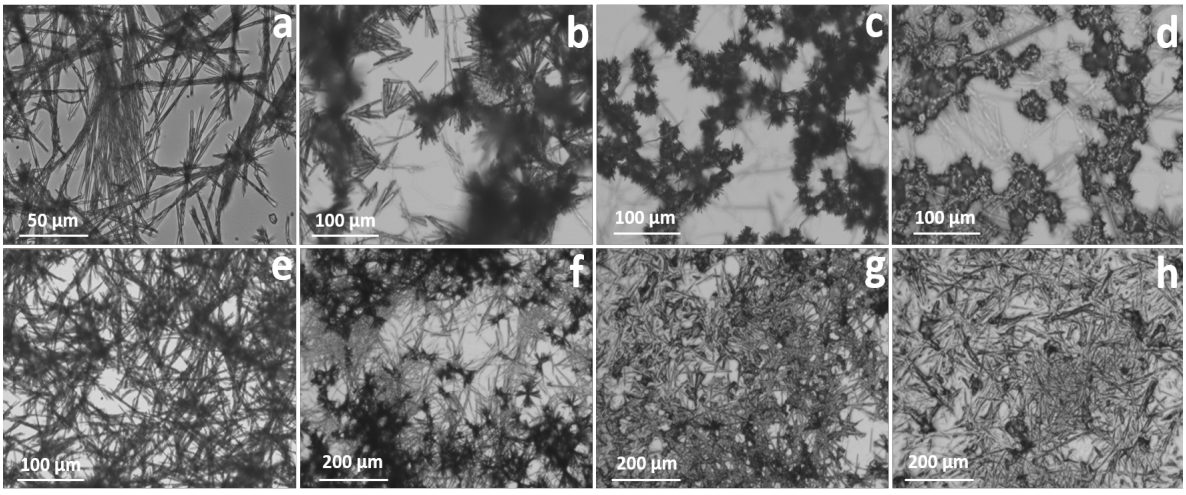

Figure S20: Microscopy images of **FmocV** under when co-incubated with tannic acid (a) **FmocV** at 9 mM at room temperature under bright field; (b) at 9 mM with tannic acid 1:1 at room temperature; (c) at 9 mM with tannic acid 1:3 at room temperature; (d) at 9 mM with tannic acid 1:5 at room temperature; (e) **FmocV** after heating under bright field; (b) with tannic acid 1:1 after heating; (c) with tannic acid 1:3 after heating; (d) with tannic acid 1:5 after heating

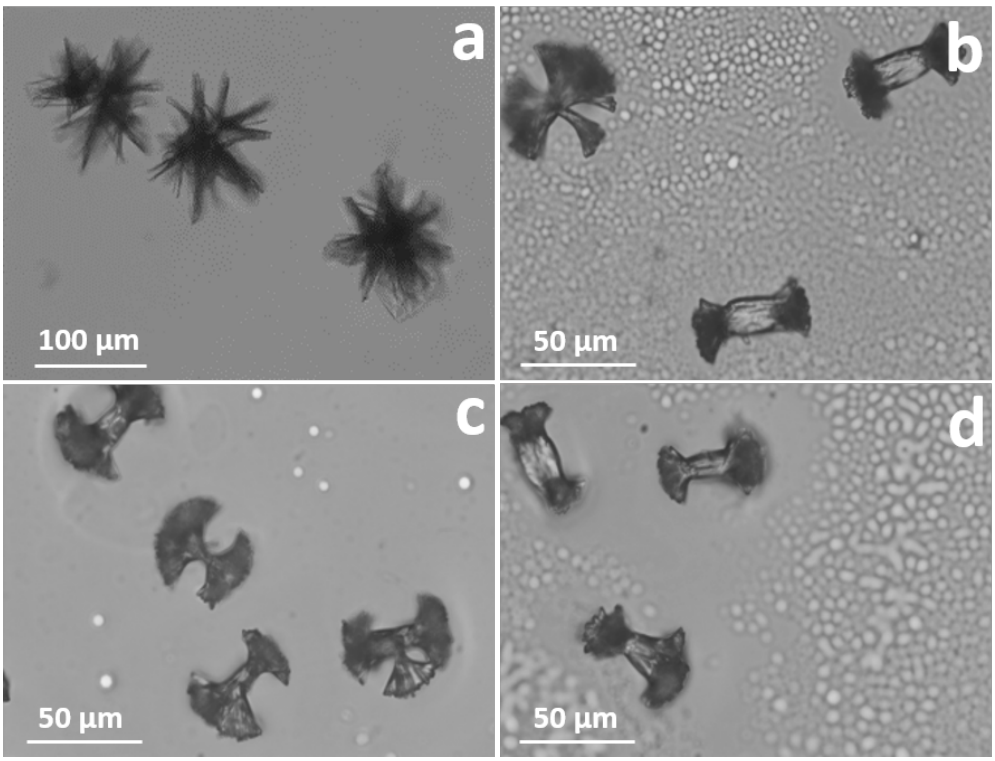

Figure S21: Microscopy images of **FmocL** at 3 mM concentration under room temperature when co-incubated with tannic acid. (a) **FmocL** at 3 mM under bright field; (b) with tannic acid 1:1; (c) with tannic acid 1:3; (d) with tannic acid 1:5.

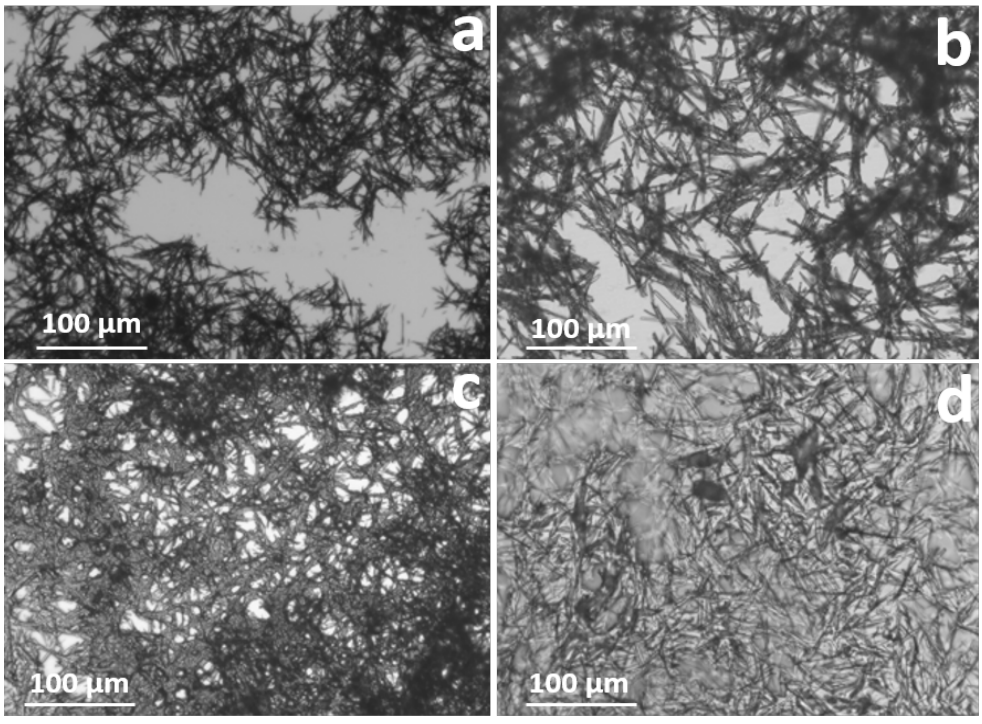

Figure S22: Microscopy images of **FmocI** at 3 mM concentration under room temperature when co-incubated with tannic acid. (a) **FmocI** at 3 mM under bright field; (b) with tannic acid 1:1; (c) with tannic acid 1:3; (d) with tannic acid 1:5.

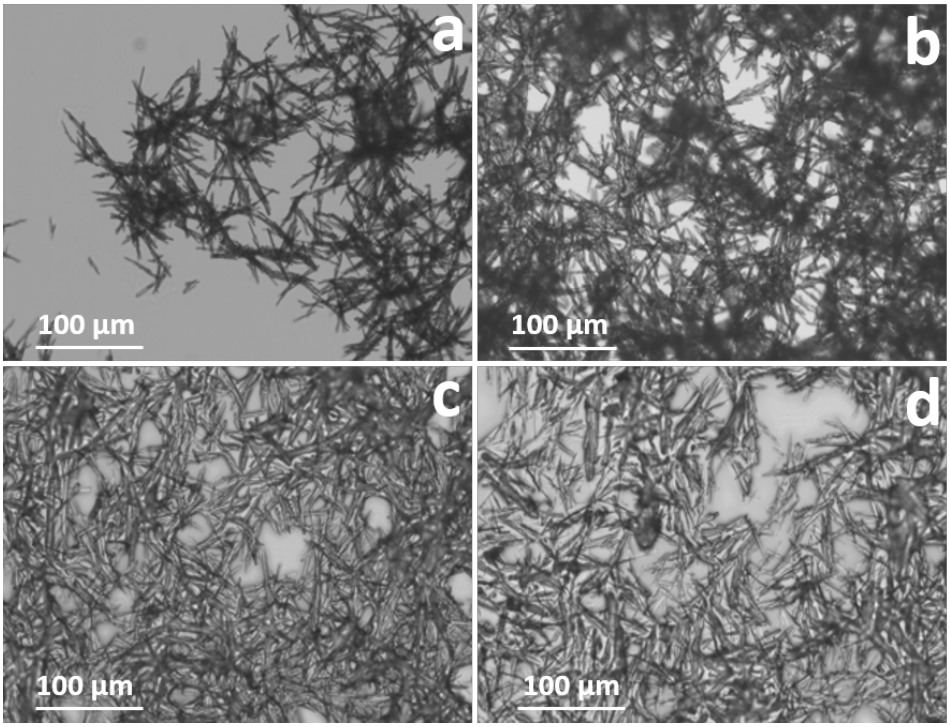

Figure S23: Microscopy images of **FmocI** at 3 mM concentration after heating when co-incubated with tannic acid. (a) **FmocI** at 3 mM under bright field; (b) with tannic acid 1:1; (c) with tannic acid 1:3; (d) with tannic acid 1:5.

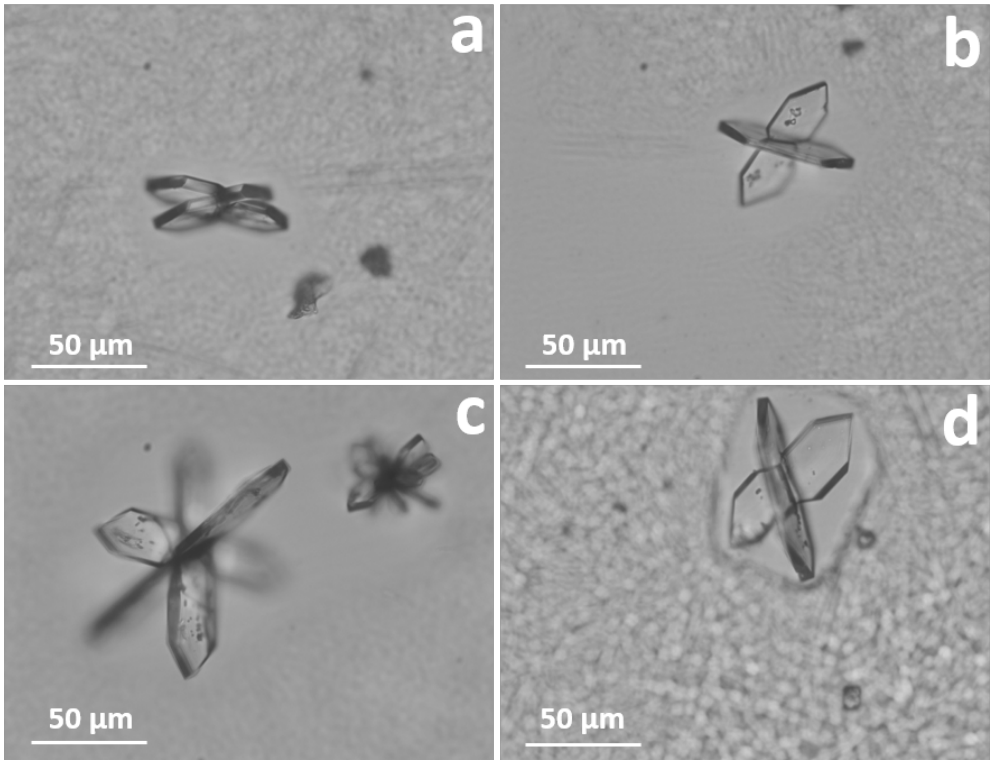

Figure S24: Microscopy images of **FmocA** at 3 mM concentration under room temperature condition when co-incubated with urea. (a) **FmocA** at 3 mM under bright field; (b) with urea 1:1; (c) with urea 1:3; (d) with urea 1:5.

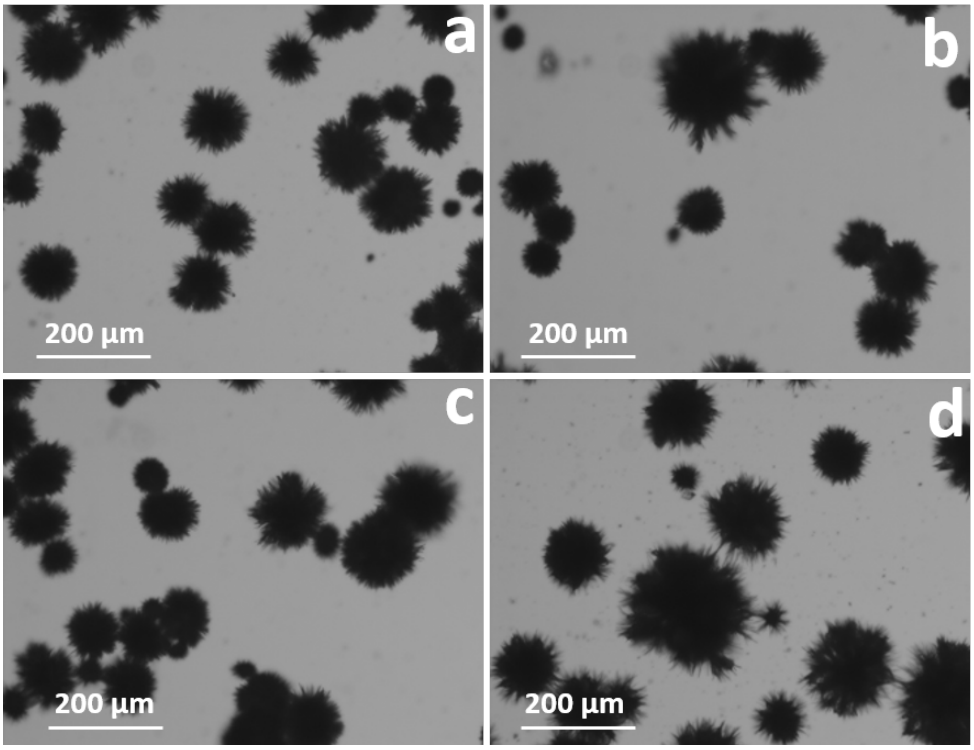

Figure S25: Microscopy images of **FmocV** at 5 mM concentration under room temperature condition when co-incubated with urea. (a) **FmocV** at 5 mM under bright field; (b) with urea 1:1; (c) with urea 1:3; (d) with urea 1:5.

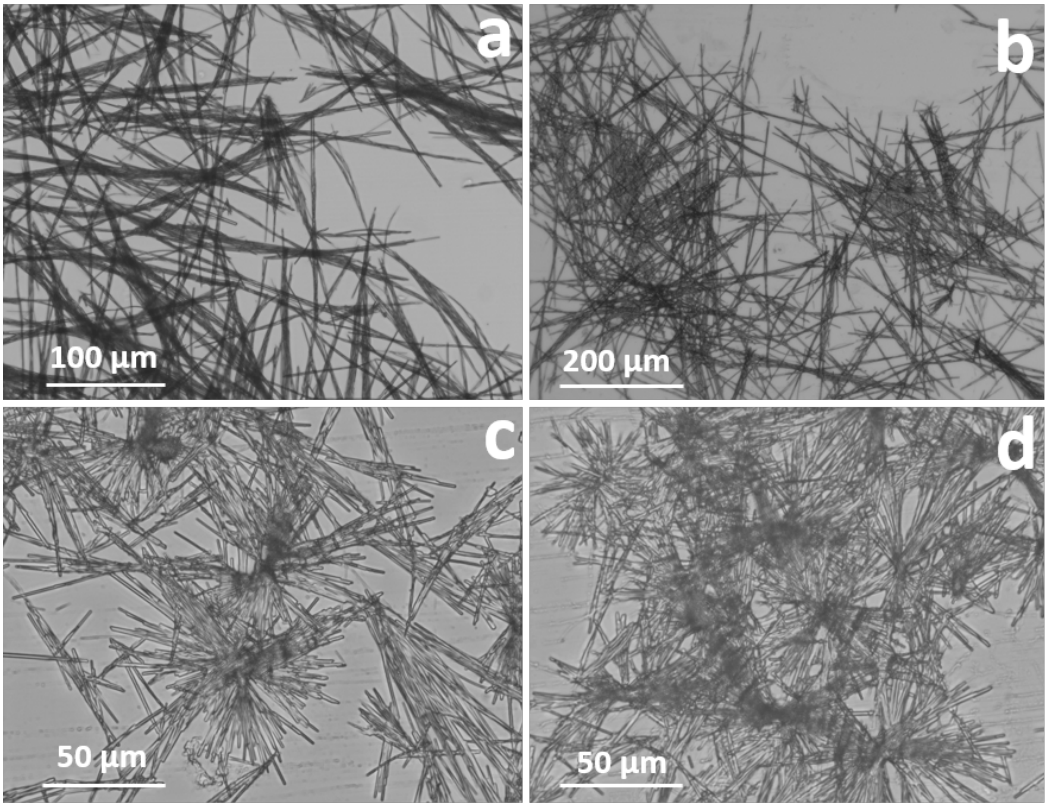

Figure S26: Microscopy images of **FmocV** at 9 mM concentration under room temperature condition when co-incubated with urea. (a) **FmocV** at 9 mM under bright field; (b) with urea 1:1; (c) with urea 1:3; (d) with urea 1:5.

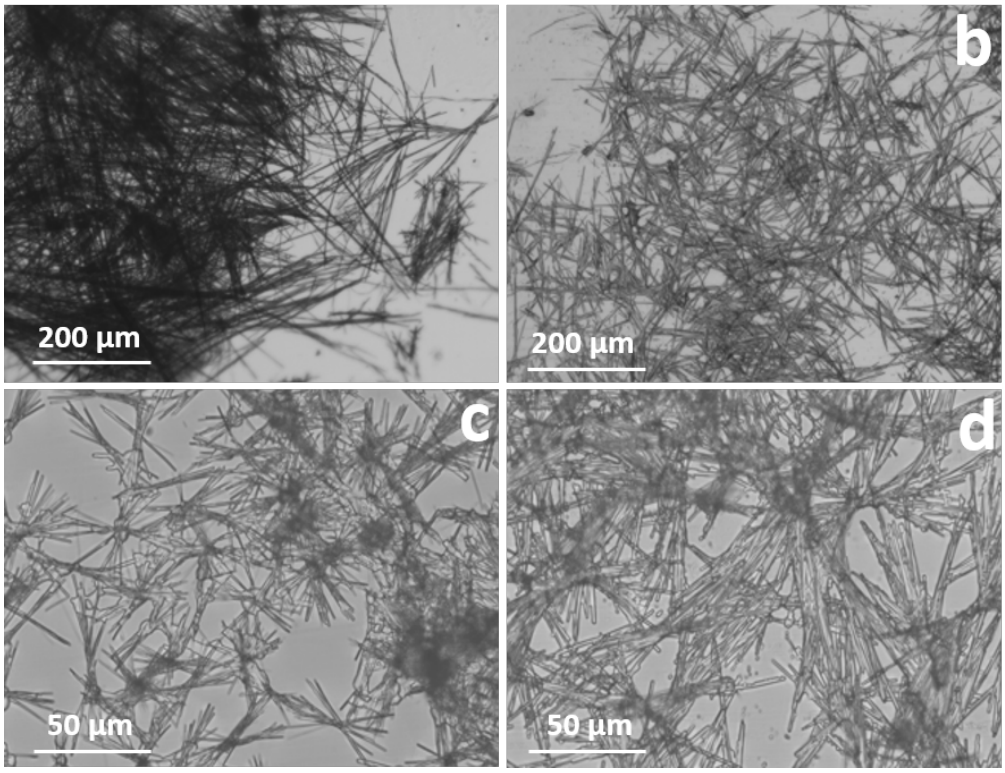

Figure S27: Microscopy images of **FmocV** at 3 mM concentration after heating when co-incubated with urea. (a) **FmocV** at 3 mM under bright field; (b) with urea 1:1; (c) with urea 1:3; (d) with urea 1:5.

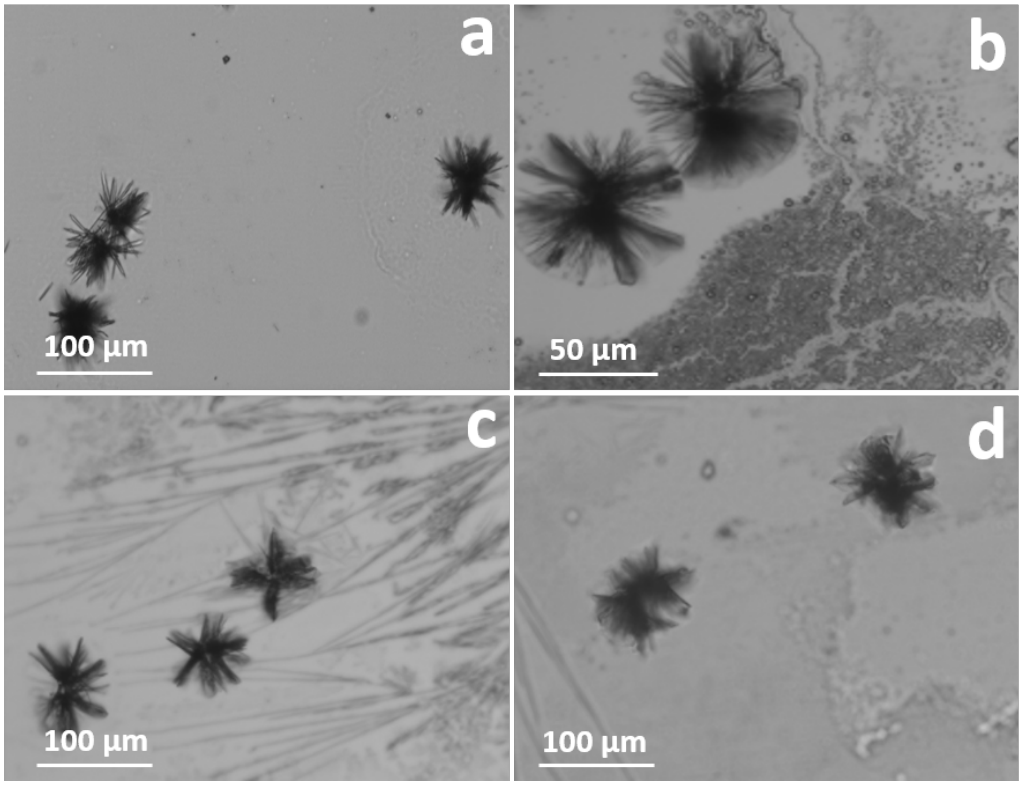

Figure S28: Microscopy images of **FmocL** at 3 mM concentration at room temperature when co-incubated with urea. (a) **FmocL** at 3 mM under bright field; (b) with urea 1:1; (c) with urea 1:3; (d) with urea 1:5.

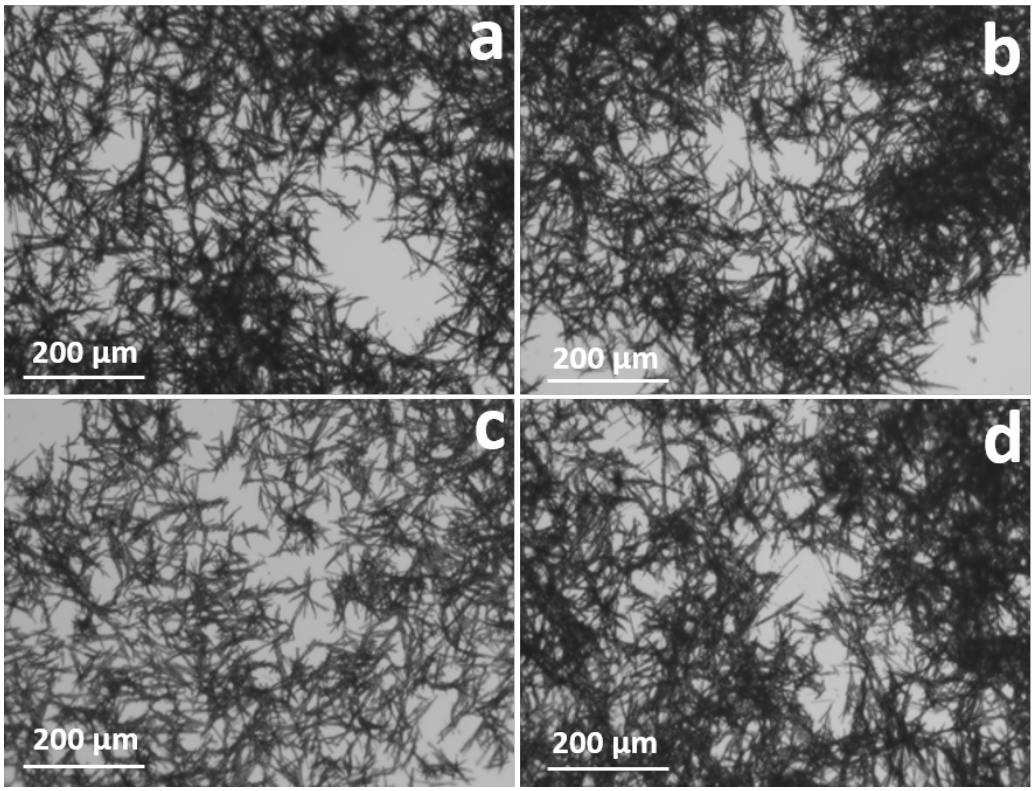

Figure S29: Microscopy images of **FmocI** at 3 mM concentration at room temperature when co-incubated with urea. (a) **FmocI** at 3 mM under bright field; (b) with urea 1:1; (c) with urea 1:3; (d) with urea 1:5.

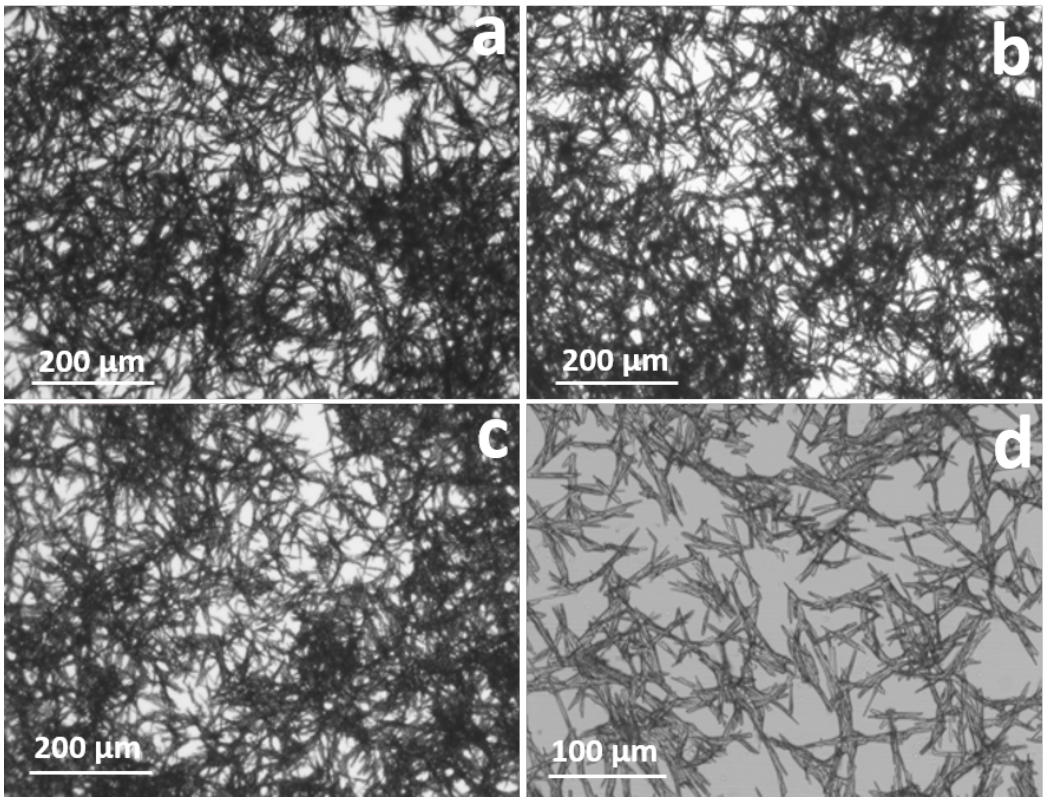

Figure S30: Microscopy images of **FmocI** at 3 mM concentration after heating when co-incubated with urea. (a) **FmocI** at 3 mM under bright field; (b) with urea 1:1; (c) with urea 1:3; (d) with urea 1:5.

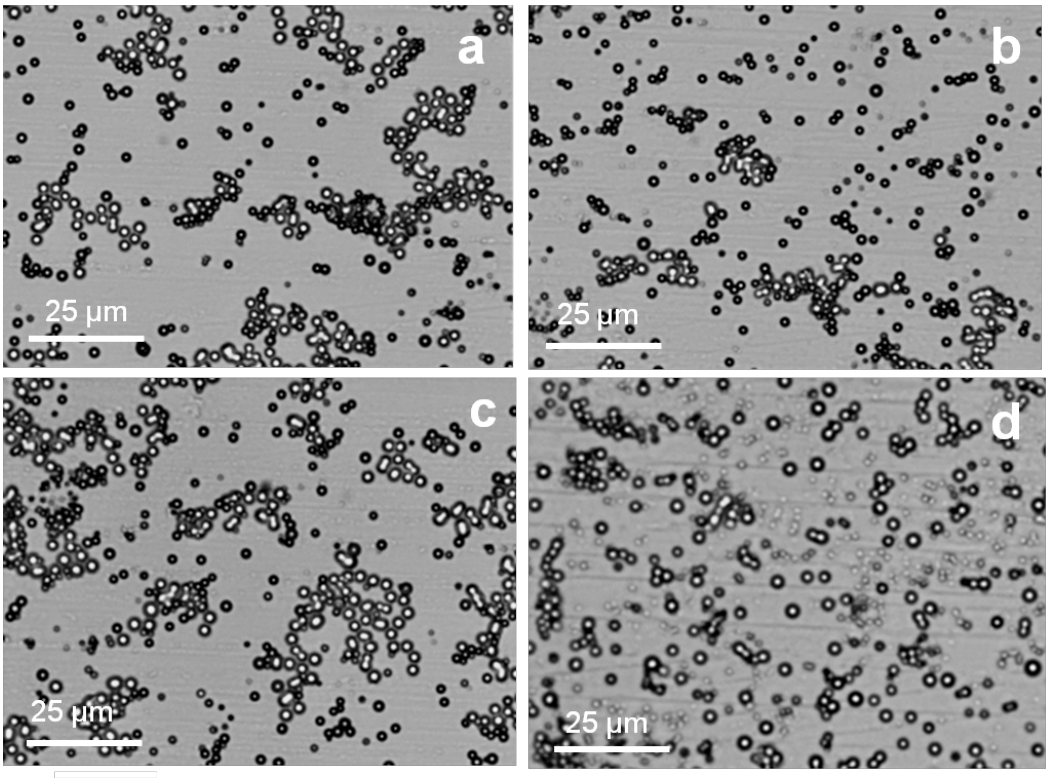

Figure S31: Microscopy images of **FmocP** at 3 mM concentration under RT when co-incubated with urea. (a) **FmocP** at 3 mM under bright field; (b) with urea 1:1; (c) with urea 1:3; (d) with urea 1:5.

pH Assembly Studies

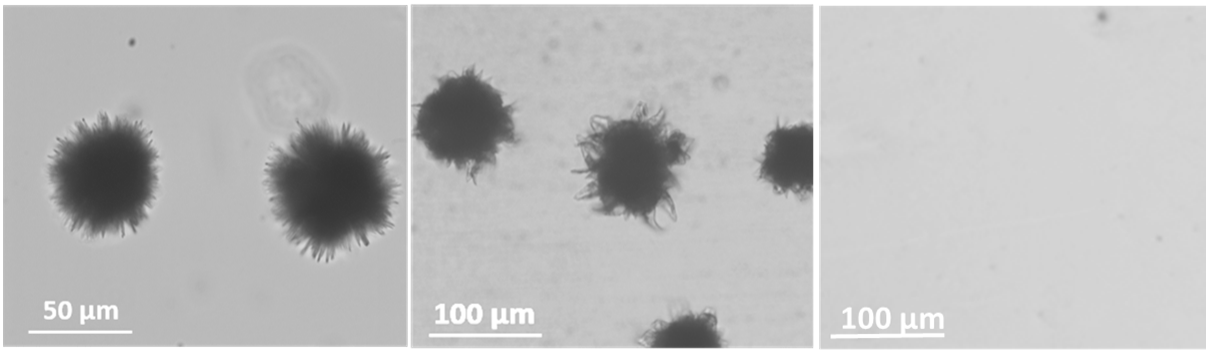

Figure S32: Microscopy images of **FmocV** at 3 mM concentration after heating condition at varied pH. (a) pH 3, (b) pH 5 and (c) pH 8.

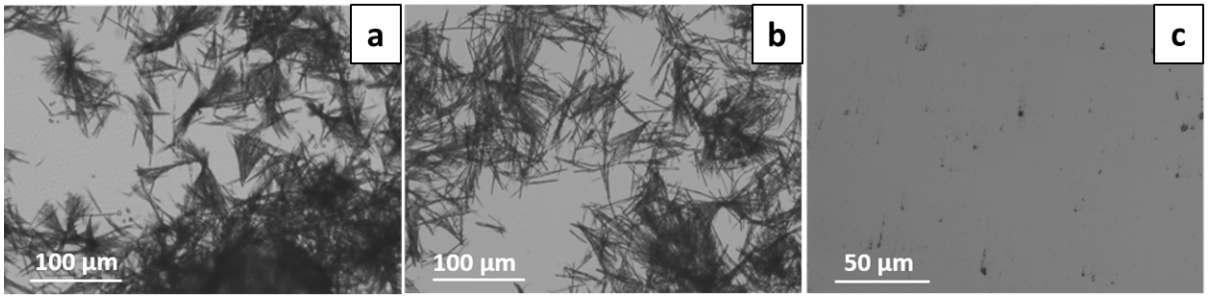

Figure S33: Microscopy images of **FmocV** at 9 mM concentration after heating condition at varied pH. (a) pH 3, (b) pH 5 and (c) pH 8.

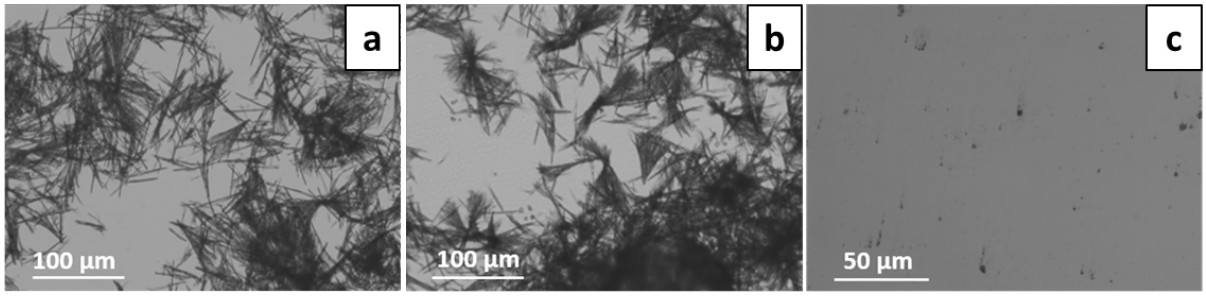

Figure S34: Microscopy images of **FmocV** at 9 mM concentration at room temperature at varied pH. (a) pH 3, (b) at pH 5; (c) at pH 8.

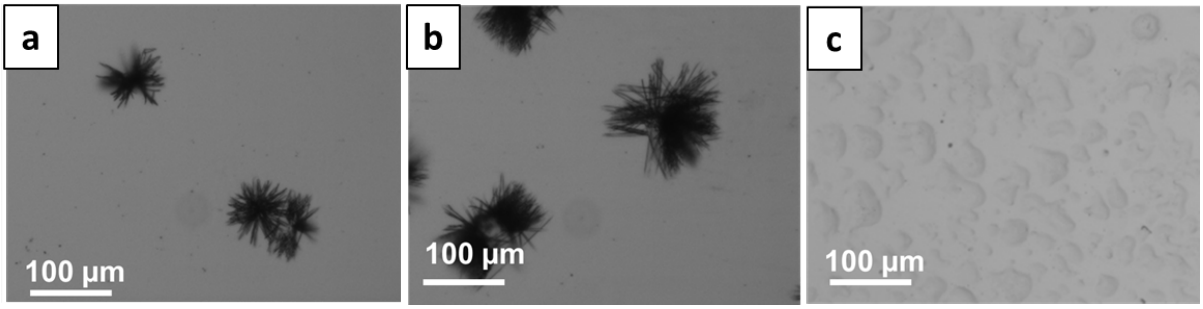

Figure S35: Microscopy images of **FmocL** at 3 mM concentration at room temperature at varied pH. (a) pH 3, (b) pH 5 and (c) pH 8.

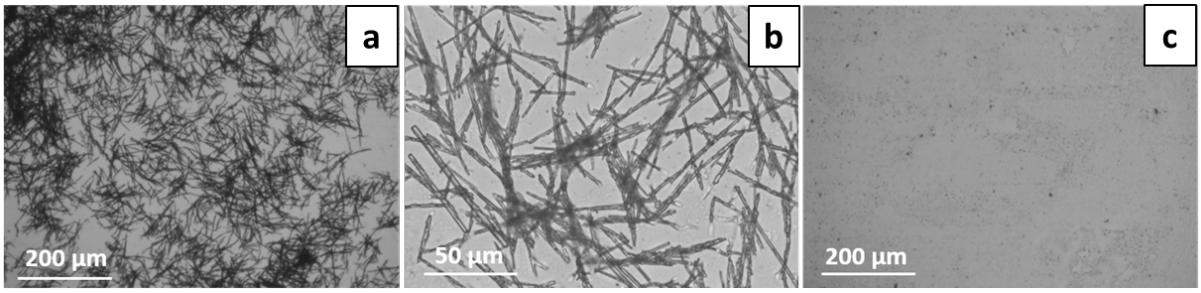

Figure S36: Microscopy images of **FmocI** at 3 mM concentration at room temperature at varied pH. (a) 3, (b) 5 and (c) 8.

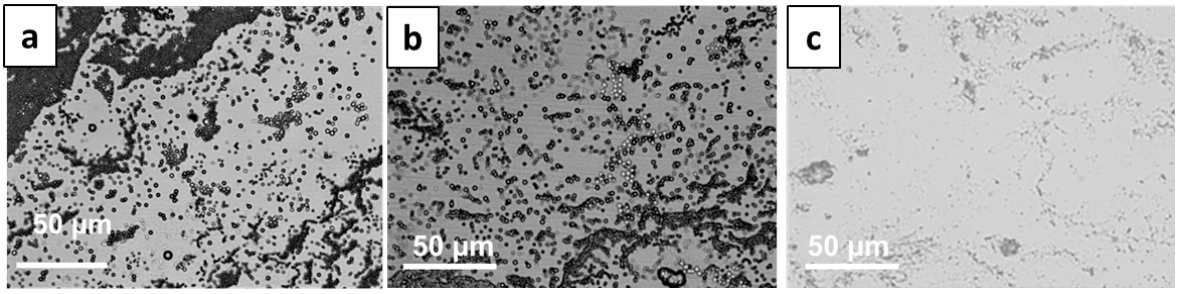

Figure S37: Microscopy images of **FmocP** at 3 mM concentration at room temperature at varied pH. (a) pH 3, (b) pH 5 and (c) pH 8.

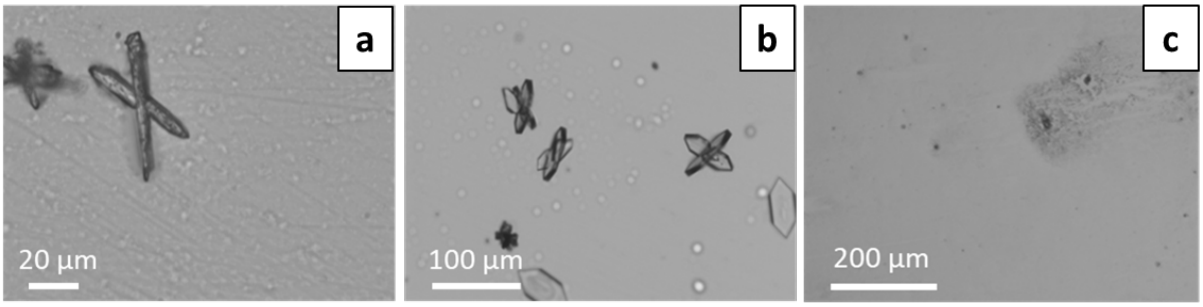

Figure S38: Microscopy images of **FmocA** at 3 mM concentration at room temperature at varied pH. (a) pH 3, (b) pH 5 and (c) pH 8.

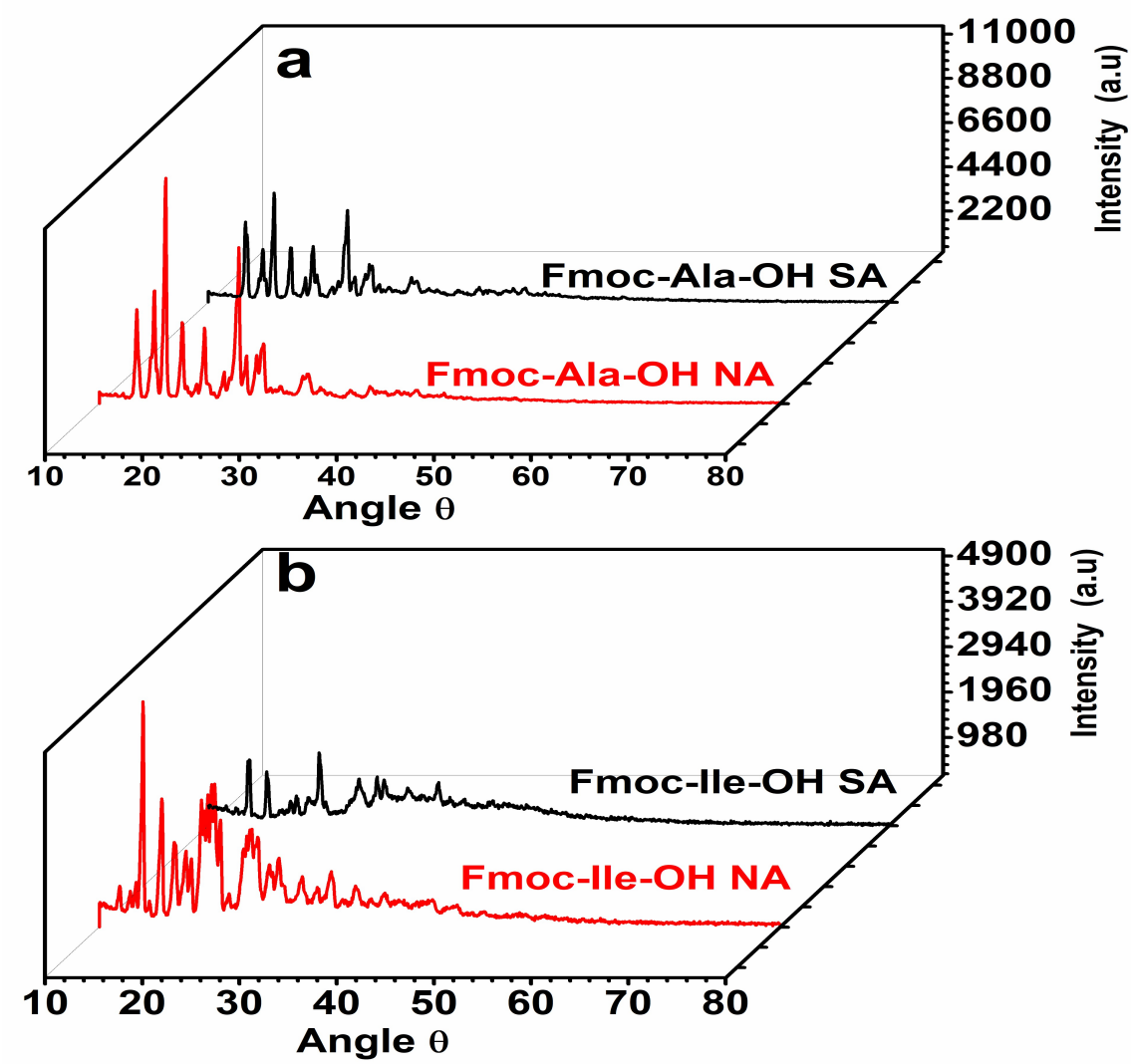

Figure S39: The comparative XRD diffractogram of **FmocA** non-assembled **(NA)** and **FmocA** self-assembled **(SA)** suggest the XRD peaks are intact and the crystalline nature is retained even after self-assembly. In **FmocI** however the peaks are broadened and some peaks also disappear after self-assembly indicating a change in molecular packing and a transition from crystalline to an amorphous state.

XRD Analysis

To better understand the internal structure of the molecular assemblies observed we performed XRD analysis on **FmocA** and **FmocI**. These were selected to represent the two 'kinds of assembly' observed for the aliphatic Fmoc-SAAs, specifically crystals and soft amorphous fibres. These assemblies are also stable with respect to varied concentration and temperature.

To elucidate the assembly process for these representatives, XRD analysis was performed on **FmocA** and **FmocI** powder was done before and after self-assembly process (Fig. S39a). The

XRD data for **FmocA** suggest its crystalline nature is retained both before and after self-assembly as evident by shard diffraction peaks obtained in XRD in both the cases. For **FmocI** the preassembly powder was revealed to be crystalline, however the XRD spectrum became amorphous after assembly (Fig. S39b).

NMR Analysis

Solution-state ^{1}H-NMR spectroscopy is also a very useful technique to understand the aggregation process of compounds and the molecular interactions like π - π stacking which will cause change in the electron density around the proton nuclei leading to changes in chemical shift and slight peak shifts in NMR. The process of self-assembly is mediated by non-covalent interactions such as π - π stacking, hydrogen bonding, electrostatic interactions, hydrophobic attractions etc. Hence, the solution state ^{1}H-NMR studies of **FmocA** were studied as the representative for all Fmoc modified aliphatic single amino acids at 1, 3, 5, 7 and 9 mg/mL in DMSO d_6. The DMSO d_6 solvent system was chosen since the Fmoc-amino acids were soluble in it and for NMR analysis turbid solution (as used for microscopy) cannot be used.

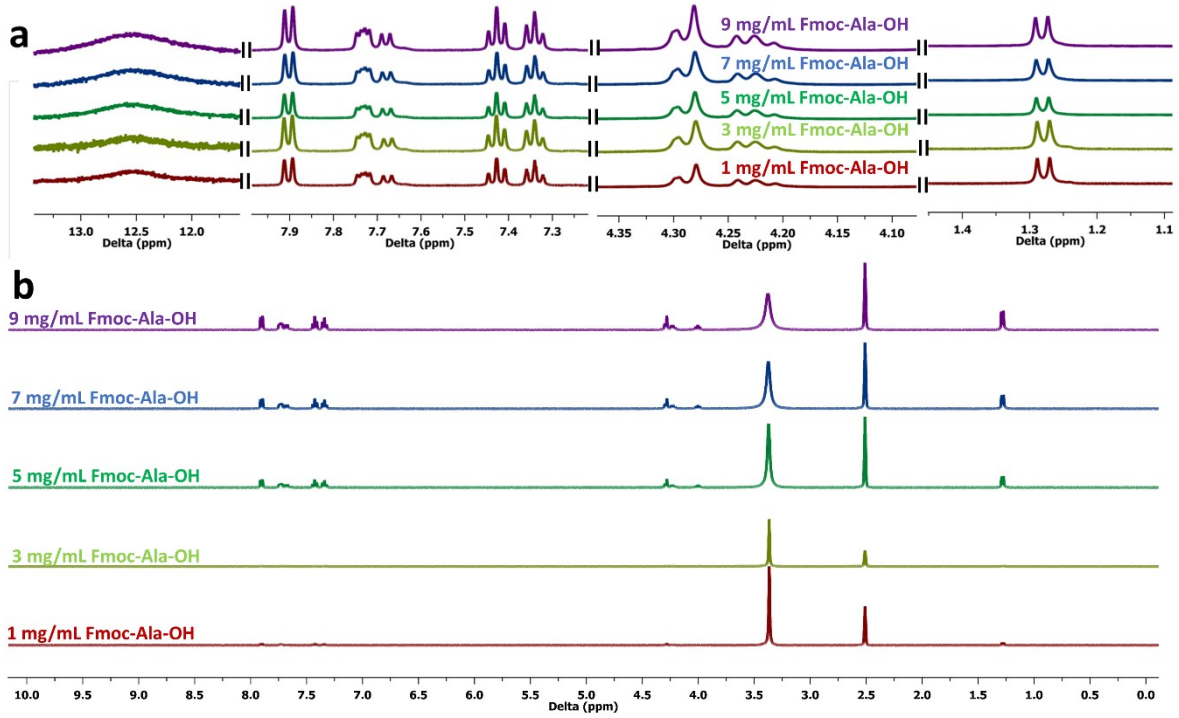

Figure S40: ^{1}H NMR spectra of **FmocA** at various concentrations (a) expansion of **FmocA** ^{1}H NMR spectra; (b) Full ^{1}H NMR spectra of **FmocA** in DMSO-d_6.

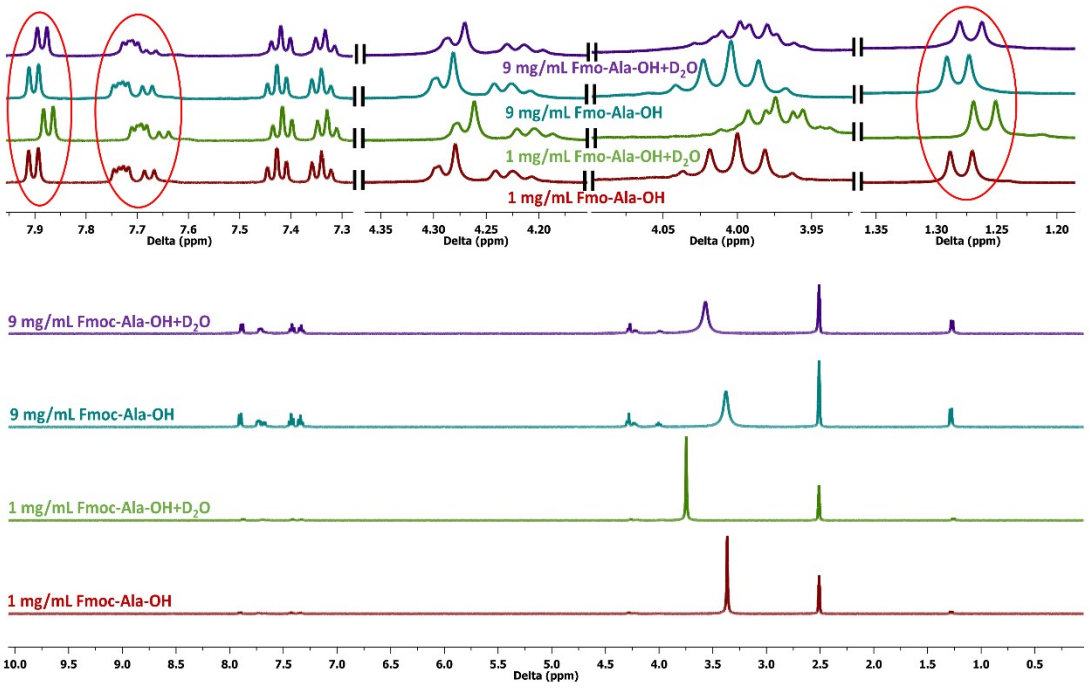

Figure S41: (a) Expansion of **FmocA** ^{1}H NMR spectra with and without D_2O at 1 and 9 mg/mL; (b) Full ^{1}H NMR spectra of **FmocA** with and without drop of D_2O at 1 and 9 mg/mL.

The concentration-dependent solution-state ^{1}H-NMR spectroscopy studies on **FmocA** suggest that as the concentration is increased, there is no up field shift. This indicated that there is no aggregation formed in DMSO-d_6 solvent due to the high solubility of **FmocA** in DMSO. On increasing the concentration, it promotes the close packing of **FmocA**. The study demonstrates that on increasing the concentration of **FmocA** from 1 to 9 mg/mL, peak broadening occurs due to the enhancement in intermolecular interactions such as hydrogen bonding. On the other hand, protons of the carbamate (-NH) and acid (-COOH) functional groups exhibit no shifting which also demonstrated that the self-assembled structure is absent in DMSO-d_6 (Fig. S40a and S41a).

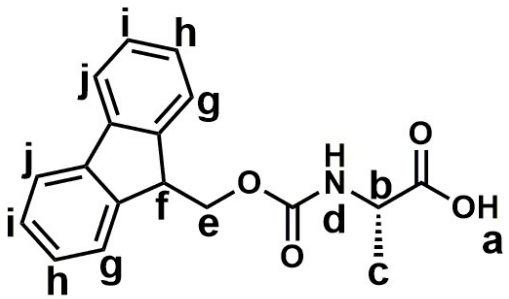

The different protons present in **FmocA** are denoted as **a** to **j**. At concentration 1 mg/mL, the chemical shift of proton **a** is attributed at 12.50 ppm, while the **b** proton peak could be assigned at 4.04-3.36 ppm as multiplet. Doublet **c** protons of methyl group exhibit the signal in the range of 1.29-1.27 ppm. Signals in the range of 7.69-7.67 ppm were assigned to carbamate -NH doublet **d** protons. On the other hand, **e** proton peak is assigned in the range of 4.30-4.28 ppm and this proton displays doublet multiplicity. Signal at 4.24-4.21 ppm was assigned to **f** protons and these protons show triplet multiplicity. Remaining four signals at 7.91-7.89 7.75-7.72, 7.45-7.41 and 7.36-7.32 ppm were attributed to **g**, **h**, **i,** and **j** protons with multiplicity of doublet, quartet, triplet, and triplet respectively.

Since the **FmocA** is highly soluble in DMSO-d_a solvents to induce the formation of aggregates in the DMSO-d_6 solvents system we added drop of D_2O in DMSO-d_6 at 1 mg/mL and 9 mg/mL concentrations. The study demonstrated that after the addition of D_2O the aromatic protons become more shielded due to the shielding effect in which the ring current of the adjacent aromatic rings is produced by the π - π stacked aggregates. Surprisingly the methyl protons of **FmocA** shows the upfield shifting due to the more hydrophobic interactions on addition of drop of D_2O which could be due to the formation of more aggregates caused by the π - π stacking in DMSO-d6 and D_2O system (Figure S42).

Since D_2O has only 1% H_2O, hence, to understand the role of water more precisely, higher concentration (9mg/mL) of **FmocA** as representative system was used and increasing % of water added. Indeed, we could observe more prominent upfield peak shift throughout the spectra indicating due to the hydrophobic nature of Fmoc-SAAs the pi-pi stacking interactions are facilitated as increasing % of H_2O was added.

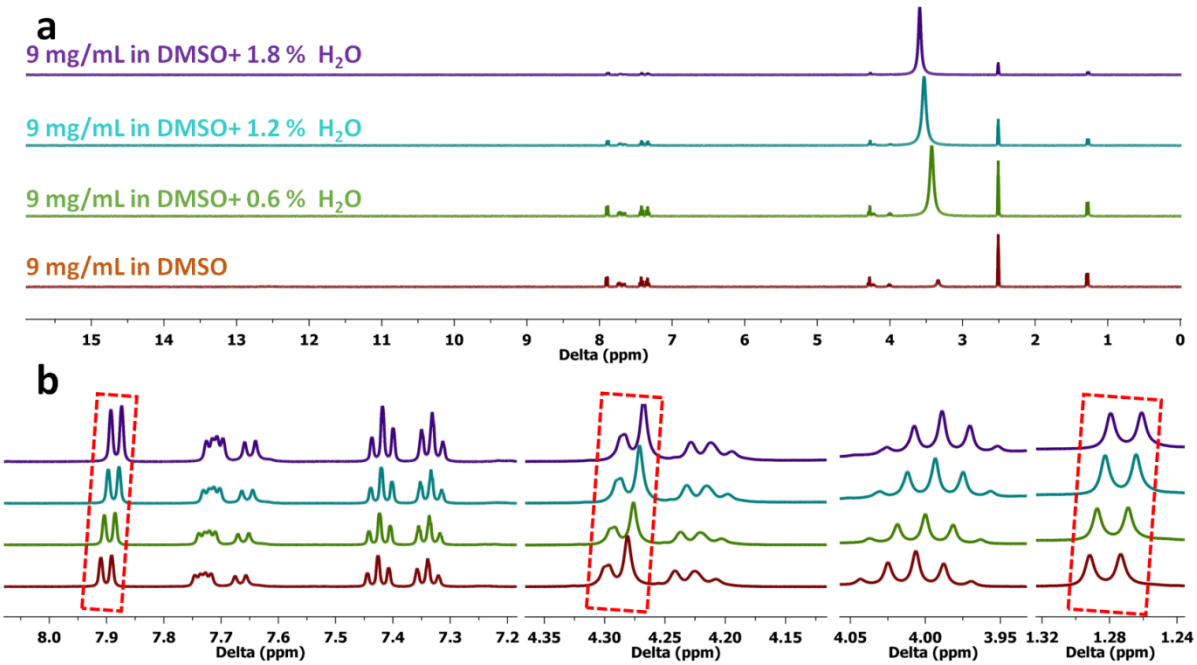

Figure S42: Solution state ^{1}H NMR of FmocA under varying % of water indicates increased pi-pi stacking interactions (as up field shift) as% of water is increased

Further, to study the effect of temperature the solution state ^{1}H NMR of **FmocA** (9mg/mL) was also recorded under varying temperature which reveal both pi-pi stacking as well as hydrogen bonding interactions are increasing as temperature is increased since a upfield peak shift is observed in aromatic region which indicates pi-pi stacking while downfield peak shift occurs in aliphatic region which corresponds to intermolecular hydrogen bonding (Figure S43).

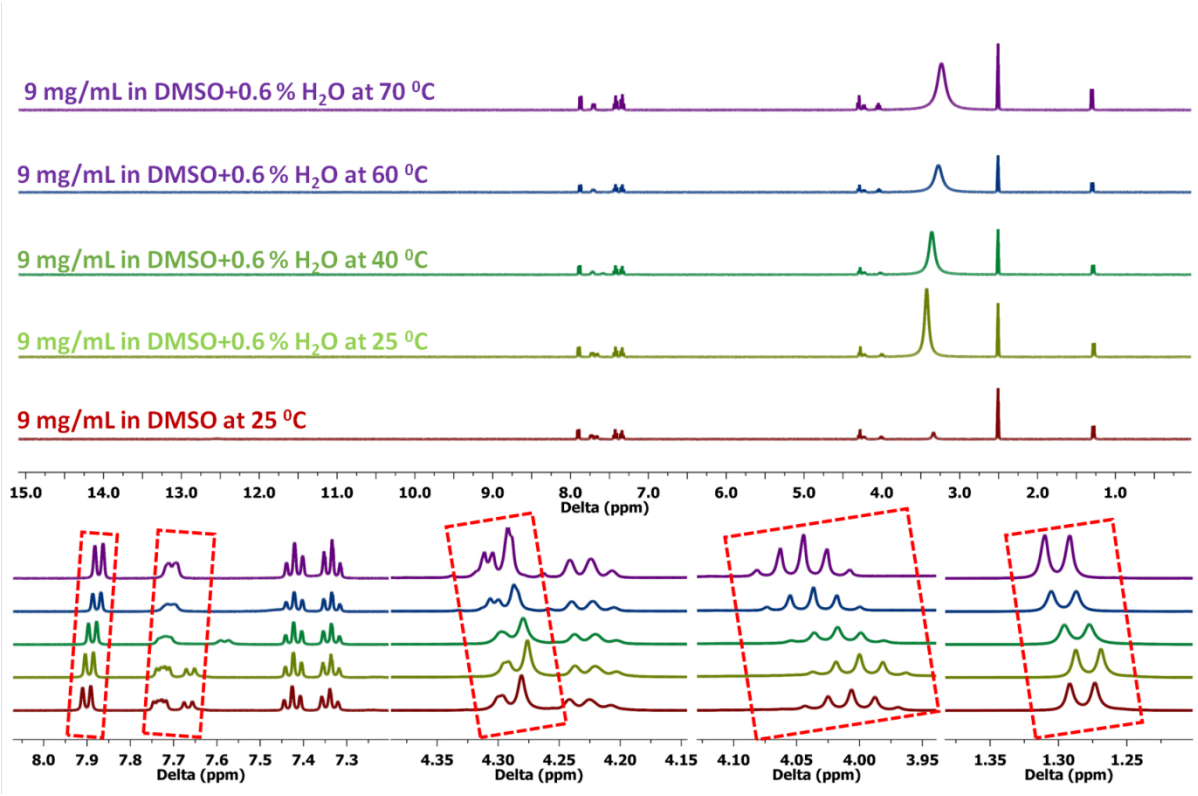

Figure S43: Solution state ^{1}H NMR of **FmocA** under varying temperature with added 0.6% water to study its effect indicates both pi-pi stacking as well as hydrogen bonding interactions are enhanced as temperature increase.

Methanol:Water studies

To understand the formation of crystalline self-assembled structures as observed for **FmocA** and **FmocL** in Figure 2**,** the self-assembly of different Fmoc-SAAs were also analysed under varying % of methanol: water. The self-assembled structures illustrated in Figure 2 were studied in water: methanol solvent system wherein the % of methanol was only 10 – 20% and the self-assembly was assessed in predominantly aqueous environments. **Fmoc-SAAs** were soluble in methanol and water was the incompatible solvent which induced aggregation. Hence, to understand the effect of solubility parameters on self-assembly it was necessary to study 3mM **Fmoc-SAAs** under varying% of water: methanol (0-90%).

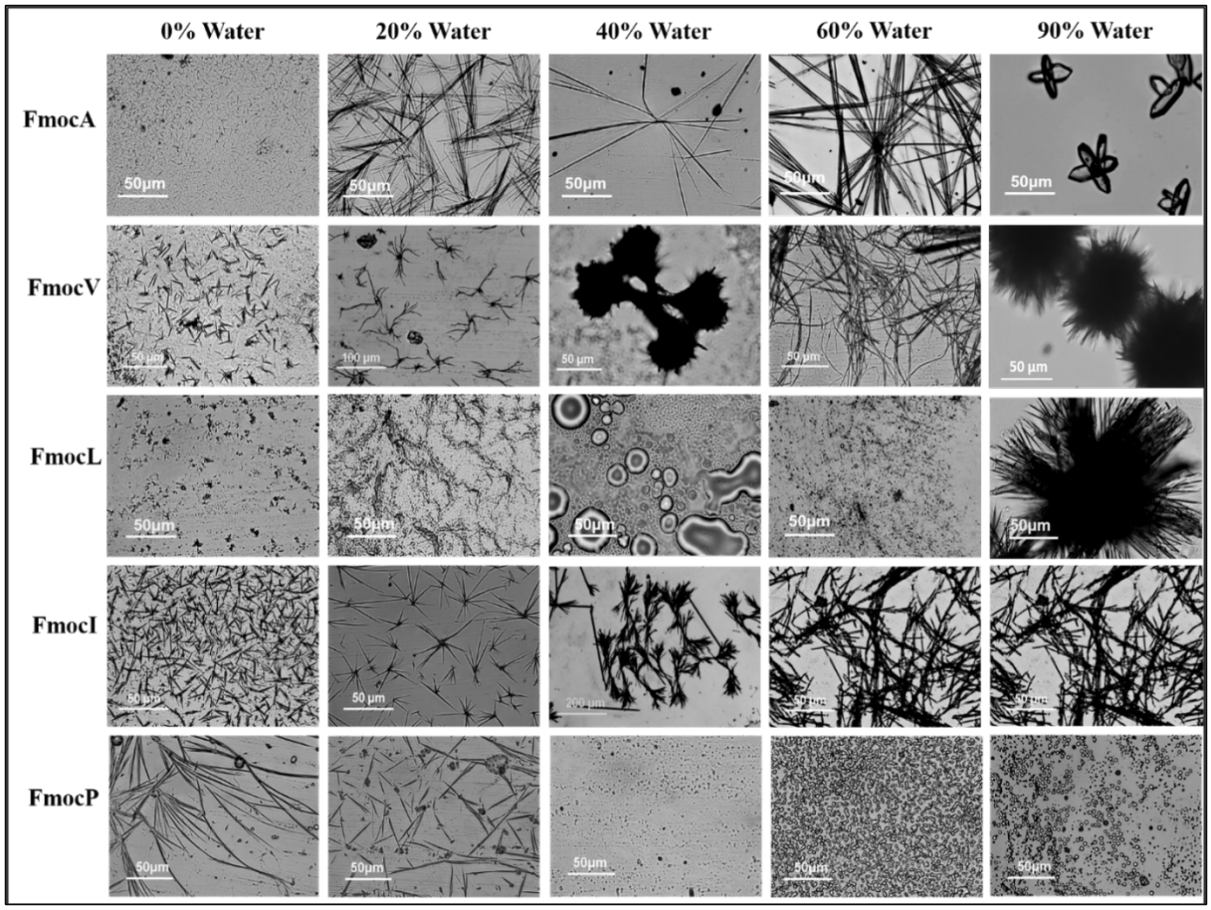

Figure S44: The optical microscopy images of 3mM **Fmoc-SAAs** under varying % of water in methanol.

Interestingly, **Fmoc-SAAs** revealed morphological transitions which suggested crucial role of solubility in determining the crystalline characteristic of the self-assemblies formed. **FmocA** which assembles to crystalline flowers as observed in Figure 2, self-assembles to yield non crystalline fibrillar assemblies as the percentage of methanol (a more soluble solvent was increased. From the microscopy studies of FmocA it is evident that it solubilize in 100% methanol and as water is added it gradually changes to fibres or tubes like assemblies till 60% water. A further addition of water triggers formation of crystalline flower as observed in Figure 2 of **FmocA** (Figure 4). **FmocV** assemble to small fibres in pure methanol. As the water percentage is increased to aggregation behaviour changes and it form fibrous dumb-bell like morphologies at 40% which gradually change to fibers and fibrous balls as observed in Figure at higher ratio of water. Similarly, **FmocL** gets dissolved in 100% methanol and some sphere like globular structures could be observed which gradually changed to semi-crystalline flowers as observed in Figure 2 at above 90% water. Interestingly when **FmocL** dissolved in pure methanol was heated it charged soft spherical structures uniformly (Figure S16). **FmocI**

also assembled to thick fibrillar network gradually as more water was added. Interestingly. **FmocP** assembles to fibers in methanol and as water was gradually added they transformed to spherical shape which may be due to enhancement in hydrophilicity (Figure 3, S17). Hence, it may be surmised that the solubility parameters play a crucial role in driving the morphological characteristics of Fmoc-SAAs.

References

1. L. Monticelli, S. K. Kandasamy, X. Periole, R. G. Larson, D. P. Tieleman and S. J. Marrink, *J. Chem. Theory Comput*, 2008, **4**, 819-834.
2. A. van Teijlingen, H. W. A. Swanson, K. H. A. Lau and T. Tuttle, *J. Phys. Chem. Lett.*, 2022, **13**, 4046-4051.
3. G. Campos-Villalobos, F. R. Siperstein and A. Patti, *Mol. Syst. Des. Eng.*, 2019, **4**, 186-198.
4. D. H. de Jong, G. Singh, W. F. D. Bennett, C. Arnarez, T. A. Wassenaar, L. V. Schafer, X. Periole, D. P. Tieleman and S. J. Marrink, *J. Chem. Theory Comput*, 2013, **9**, 687-697.
5. J. S. Hub, B. L. de Groot and D. van der Spoel, *J. Chem. Theory Comput*, 2010, **6**, 3713-3720.
6. Martini tutorials: Free energy techniques, http://md.chem.rug.nl/index.php/tutorials-general-introduction-gmx5/partitioning-techniques#ThermodynamicIntegration, Accessed (05/05/2022).
7. S. J. Marrink, L. Monticelli, M. N. Melo, R. Alessandri, D. P. Tieleman and P. C. T. Souza, *Wiley Interdiscip. Rev. Comput. Mol. Sci.*, 2022.
8. H. Bekker, H. J. C. Berendsen, E. J. Dijkstra, S. Achterop, R. Vondrumen, D. Vanderspoel, A. Sijbers, H. Keegstra, B. Reitsma and M. K. R. Renardus, *Physics Computing '92*, 1993, 252-256.
9. W. Humphrey, A. Dalke and K. Schulten, *J Mol Graph Model*, 1996, **14**, 33-38.
10. N. Michaud-Agrawal, E. J. Denning, T. B. Woolf and O. Beckstein, *J. Comput. Chem.*, 2011, **32**, 2319-2327.
11. D. H. de Jong, S. Baoukina, H. I. Ingolfsson and S. J. Marrink, *Comput. Phys. Commun.*, 2016, **199**, 1-7.